TECHNISCHE UNIVERSITÄT WIEN

Impact of a driven right leg electrode to reduce signal noise in a low-cost EEG

DIPLOMARBEIT

zur Erlangung des akademischen Grades
Diplom-Ingenieur

im Rahmen des Studiums
Biomedical Engineering

eingereicht von
Thomas Lohninger BSc.
Matrikelnummer 1126085

ausgeführt am Institut für
Analysis und Scientific Computing
Technische Universität Wien

unter der Anleitung von
Ao.Univ.Prof. Dipl.-Ing. DDDr Frank Rattay

sowie
Mag.rer.soc.oec. Dipl.-Ing. Dr.techn. Andreas Fellner

Wien, 01. Juni, 2021

Technische Universität Wien

A-1040 Wien Karlsplatz 14 Tel. +43-1-58801-0
www.tuwien.ac.at

Abstract

The EEG is a powerful and yet easy to use tool to measure the brain activity of a person. It can help analyzing reactions in the patient's brain with a high temporal resolution and without the danger that comes with the exposure to radiation or strong magnetic fields as it is the case for several other methods found in this field of research. Due to the relatively low hardware costs and the potential to build one without the need of access to high precision manufacturing facilities the EEG is of special interest in private research activities.

The aim of this thesis is to shine light on the theoretical aspects of building an EEG and the obstacles that present themselves while doing so. Furthermore, once the EEG is built, the influence of the use of a driven right leg electrode on the signal quality is shown and compared with use of a digital signal filter. This method of noise filtering is expected to produce meaningful improvements while conducting measurements. The knowledge gained from this experiment will not only provide a useful insight on creating stable measuring conditions but can also serve as a valuable foundation for further research done on the use of the EEG as a brain machine interface.

Kurzfassung

Das EEG ist ein leistungsfähiges und dennoch einfach zu bedienendes Werkzeug zur Messung der Gehirnaktivität einer Person. Es kann helfen, Abläufe im Gehirn des Patienten mit einer hohen zeitlichen Auflösung zu analysieren, ohne die Gefahr, die mit der Exposition gegenüber Strahlung oder starken Magnetfeldern einhergeht, wie es bei einigen anderen Methoden in diesem Forschungsbereich der Fall ist. Aufgrund der geringen Kosten für die Hardware und der Möglichkeit, ein solches Gerät zu bauen, ohne Zugang zu hochpräzisen Fertigungsanlagen zu haben, ist das EEG von besonderem Interesse für private Forschungsaktivitäten.

Ziel dieser Arbeit ist es, die theoretischen Aspekte des Baus eines EEGs zu beleuchten und die Hindernisse, die sich dabei ergeben, aufzuzeigen. Weiters wird nach dem Bau des EEGs der Einfluss des Einsatzes einer „driven right leg" Elektrode auf die Signalqualität aufgezeigt und mit dem Einsatz eines digitalen Signalfilters verglichen. Es wird erwartet, dass diese Methode der Rauschfilterung zu Verbesserungen bei der Durchführung der Messungen führt. Die aus diesem Experiment gewonnenen Erkenntnisse werden nicht nur einen nützlichen Einblick in die Schaffung stabiler Messbedingungen geben, sondern können auch als wertvolle Grundlage für weitere Forschungen zur Verwendung des EEG als Gehirn-Computer-Schnittstelle dienen.

TABLE OF CONTENT

List of abbreviations

Abbreviation	Definition
AC	Alternating current
ATP	Adenosintriphosphat
CAD	Computer Aided Design
CMRR	Common mode rejection ratio
CSF	Cerebrospinal fluid
DC	Direct current
DRL	Driven right leg
DSR	Dataset Ready
DTR	Data Terminal Ready
ECG	Electrocardiogram
EEG	Electroencephalography
EMG	Electromyography
ESD	Electrostatic Discharge
FFT	Fast Fourier Transformation
FIR	Finite Impulse Response
IC	Integrated Circuit
IIR	Infinite Impulse Response
PCB	Printed circuit board
RLD	Right leg driver
TTL	Transistor–transistor logic

1 THEORETICAL BACKGROUND

The base unit of the nerve tissue in our brain are Neurons. The main feature that distinguishes them from other cell types in our body is the electrical excitability and the ability to communicate with other cells via synapses.[1]

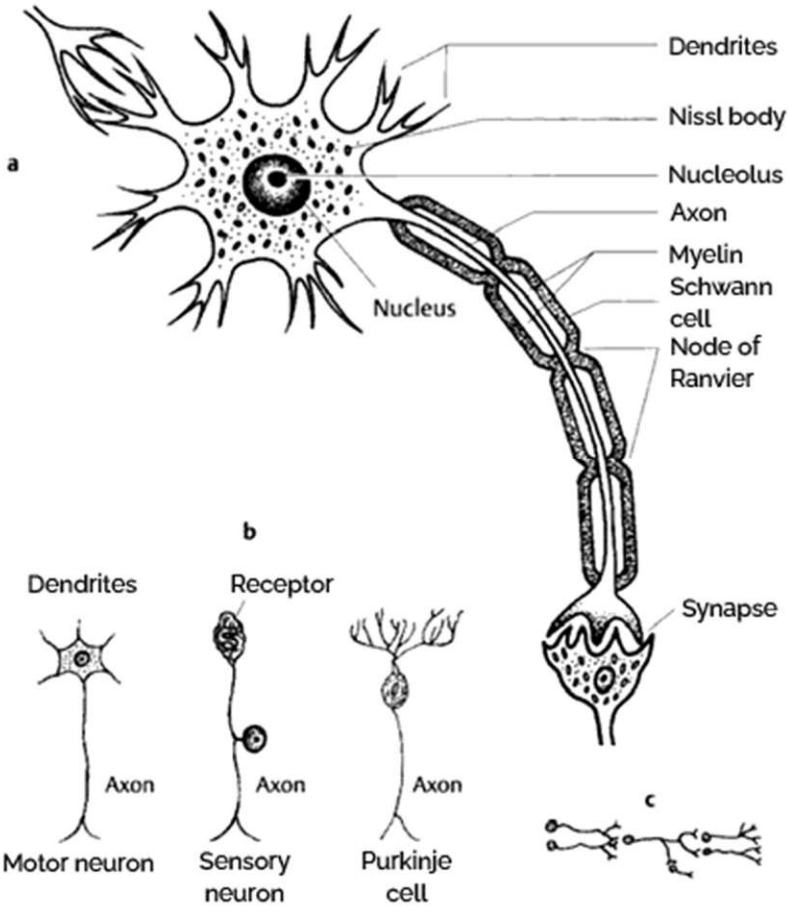

Figure 1-1 Composition of a typical neuron. From (Gertz, Schünke, & Liebman, 2003), p.2

In Figure 1-1 a typical Neuron is shown. It is composed by a cell body called Soma, multiple short elongations called Dendrites and one long elongation named Axon. The Axon is responsible for transmitting an electric pulse from the Soma to the so-called Synapse, which is a connection between two Neurons to conduct the signal to Dendrites of a neighboring Neuron. As shown in Figure 1-1c usually multiple Synapses of different cells dock with one Neuron. In addition, the Axon is also branched multiple times and transmits signals to more than one Synapsis. There are multiple different types of Neurons serving different purposes in the human body. The most common ones are illustrated in Figure 1-1 b.

The Axons of most Neurons are coated in layer of Myelin, which substantially helps conducting the electrical signals and strongly increases the speed with which the signals travels. That means that the

[1] (Gertz, Schünke, & Liebman, 2003), p.1

Neurons that lack a layer of Myelin conduct impulses significantly slower, which is the root cause of many neuropathic conditions where the Myelin sheets are destroyed over time.[2] In healthy Neurons the Myelin layer is not continuously but has small periodic gaps called nodes of Ranvier. At the nodes of Ranvier, the cell membrane is highly enriched in ion channels, allowing them to participate in the exchange of ions required to regenerate the action potential. This results in "jumps" of the action potential from node to node and allows for faster conduction.[2]

As the resting- and action-potential play a vital role in all neurophysiological processes I want to elaborate on them in the following sections.

1.1 Resting Potential

The resting membrane potential is the result of different electrostatic charges across the cell membrane. Those charges are caused by movement of many different ion types through the plasmatic membrane using various ion channels and ion pumps. Neuron cells can transition from a resting state to an excited state through excitation. The resting membrane potential is defined as the electrical potential difference across the membrane when the cell is in a non-excited state and is traditionally written as the potential difference inside the cell relative to the extracellular environment.[3]

While a lot of ions and negatively charged intracellular proteins that cannot cross the membrane contribute to the resting potential, Na+ and K+ provide the dominant influence.[3] The equilibrium potential for a single ion is calculated using the Nernst-equation:

$$V_{equ} = \frac{R\,T}{z\,F} \ln\left(\frac{c_{out}}{c_{in}}\right)$$

V_{equ}	Nernst potential [V]
R	Molar gas constant ≈ 8,314 [J/mol K]
T	Temperature[K]
z	Valence of ionic species
F	Faraday's constant ≈ 96,485 [C/mol]
C_{out}	Concentration of ions outside the membrane
C_{in}	Concentration of ions inside the membrane

Using 37°C as body temperature and changing the logarithmic base from a natural logarithm to base 10 we can simplify the equation to

[2] (Gertz, Schünke, & Liebman, 2003), p.3

[3] (Wright, 2004)

$$V_{equ} = \frac{61.5\ mV}{z} \log\left(\frac{c_{out}}{c_{in}}\right)$$

which is often found in literature. The Nernst potential for any given ionic species is the membrane potential at which the chemical and electrical gradients are equal and in opposite directions. Therefore, no flux through the membrane can occur at that potential. In a cell however the Nernst potential will never be reached as multiple permeable ions are involved and counteracting each other.[4] To consider for all the ions that are permeant through the membrane the Goldman-Hodgkin-Katz voltage equation, more commonly known as the Goldman equation, can be used:

$$V_m = \frac{RT}{F} \ln\left(\frac{\sum_i^n P_{M_i^+}[M_i^+]_{\text{out}} + \sum_j^m P_{M_j^-}[M_j^-]_{\text{in}}}{\sum_i^n P_{M_i^+}[M_i^+]_{\text{in}} + \sum_j^m P_{M_j^-}[M_j^-]_{\text{out}}}\right)$$

V_m	Membrane potential [V]
R	Molar gas constant ≈ 8,314 [J/mol K]
T	Temperature[K]
F	Faraday's constant ≈ 96,485 [C/mol]
P_{Mi}	Permeability of that ion
$[M_i]_{out}$	Concentration of ions outside the membrane
$[M_i]_{in}$	Concentration of ions inside the membrane

Again using 37°C as body temperature and changing the logarithmic base from a natural logarithm to base 10 we can simplify the equation to

$$V_{equ} = 61.5\text{mV} \log\left(\frac{\sum_i^n P_{M_i^+}[M_i^+]_{\text{out}} + \sum_j^m P_{M_j^-}[M_j^-]_{\text{in}}}{\sum_i^n P_{M_i^+}[M_i^+]_{\text{in}} + \sum_j^m P_{M_j^-}[M_j^-]_{\text{out}}}\right)$$

The most important ions involved in maintaining the resting potential are Potassium and Sodium.[5] For Potassium, a negative gradient (more intracellular than extracellular ions) and for Sodium a positive gradient are present all the time, resulting in a resting membrane potential of -70mV. As the Nernst potential for Sodium (at around +50mv) and Potassium (at around -75mV)[5] are never reached in the cell, there will be a constant influx of Sodium and outflux of Potassium through the leakage channels. To counteract this reduction of the concentration gradient the sodium-potassium pump

[4] (Kandel, Schwartz, Jessell, Siegelbaum, & Hudspeth, 2012), p.128

[5] (Kandel, Schwartz, Jessell, Siegelbaum, & Hudspeth, 2012), p.131

constantly pumps sodium outside the cell and potassium inside it using ATP in the process. This leads to a stable resting potential of around -60mV[6].

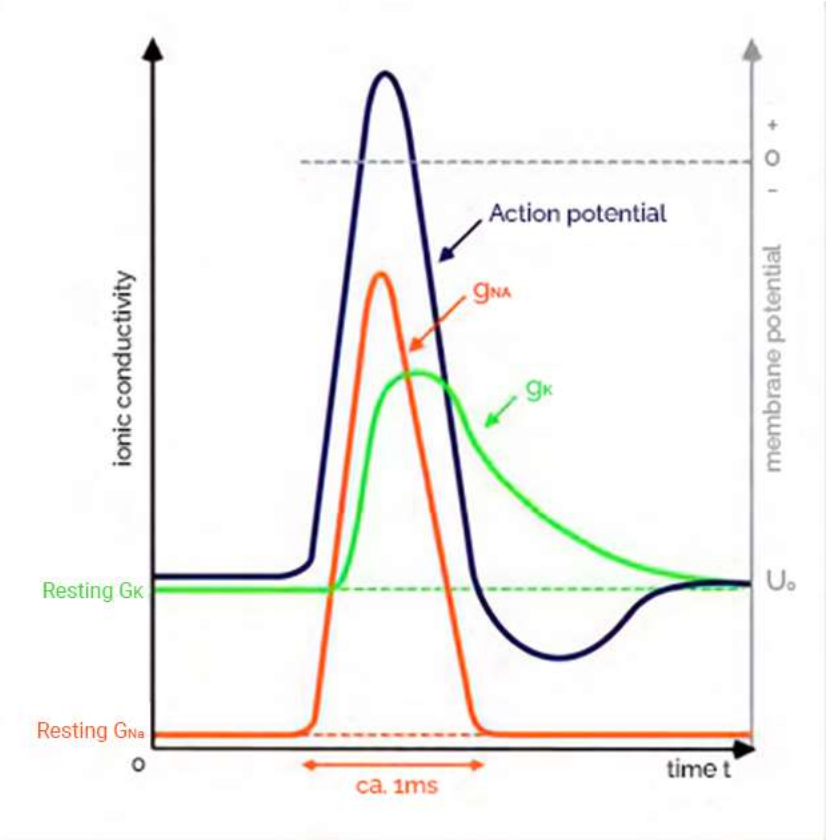

Figure 1-2 Course of the membrane potential over time. Modified after (Elsholz, Feser, & Trefzger, 2012)

1.2 Action Potential

Action potentials are temporal, characteristic deviations from the axons resting potential. In Figure 1-2 the course of the potential over time is shown. Starting with many excitatory graded potentials at the neuron's dendrites, the cells soma begins to depolarize. If this depolarization is strong enough (over -55mV) the voltage gated sodium channels at the axons are triggered to open their m-gates and let sodium flow into the intracellular space. Due to that process the permeability for the sodium ions is drastically increased and therefore according to the Goldman equation the potential of the cell will rise quickly. This process continues until the potential reaches a voltage where the h-gates of the sodium channels are closing again, and the voltage gated potassium channels are opened. This stops the influx of sodium and starts the outflow of potassium resulting in the repolarization of the axon even surpassing the membrane resting potential and hyperpolarizing the cell. After the voltage gated potassium channels are closed again the sodium-potassium pump is responsible for recreating

[6] (Kandel, Schwartz, Jessell, Siegelbaum, & Hudspeth, 2012), p.131

the initial resting potential. An action potential is an all-or-nothing reaction as it is either fully triggered or is not happening at all.[7]

In the early days of electroencephalography, the potential fluctuations measured on the surface of the skull were interpreted as superposition of the action potentials of simultaneously active brain neurons[8] since action potentials, at 120mV when measured intracellularly, represent the largest potential fluctuations of nerve cells. However their extracellularly measurable amplitude is so small that the summation of a large number of simultaneous and concurrent action potentials would be necessary to produce a measurable signal on the scalp (i.e. an EEG). With a duration of one millisecond, action potentials are much too short to be able to sum up sufficiently and therefore, the action potentials of the brain neurons cannot be the primary cause of the potential fluctuations measured in electroencephalography. While action potentials are too short lived to sum up sufficiently, postsynaptic potentials, with a duration of up to several hundred milliseconds, can produce measurable potential fluctuations on the scalp of around 50-100 microvolts. [9] This topic will be discussed further in section 2.

As mentioned earlier, the neurons in the brain are interconnected through synapses which enables communication between the individual neurons. Also, during the synaptic transmission of excitation there are spatially and temporally limited potential fluctuations, which will be described in more detail in the following, since they are one major cause of the signals recorded in the electroencephalogram.

1.3 Synaptic and postsynaptic excitation

In general, there are basically two different types of synapses: Chemical synapses, which transmit excitation by means of a purely chemical process, and electrical synapses. However, since chemical synapses are predominant in the human nervous system[10], I will focus only on chemical synapses in the following explanations.

[7] (Reece, et al., 2014), p. 1069

[8] (Zschocke & Hansen, 2012), p.2

[9] (Kirschstein, 2008)

[10] (Thompson, 1994), p.93

The transmission of excitation at a chemical synapse is shown in Figure 1-3: If an action potential conducted via the axon reaches the presynapse, the opening of specific ion channels initially leads to an increased permeability of the presynaptic membrane for Ca^{2+} ions [11]. The resulting influx of calcium ions into the intracellular area results in a movement of synaptic vesicles towards the presynaptic membrane. The vesicles store transmitter molecules (Tr) specific to the cell and release

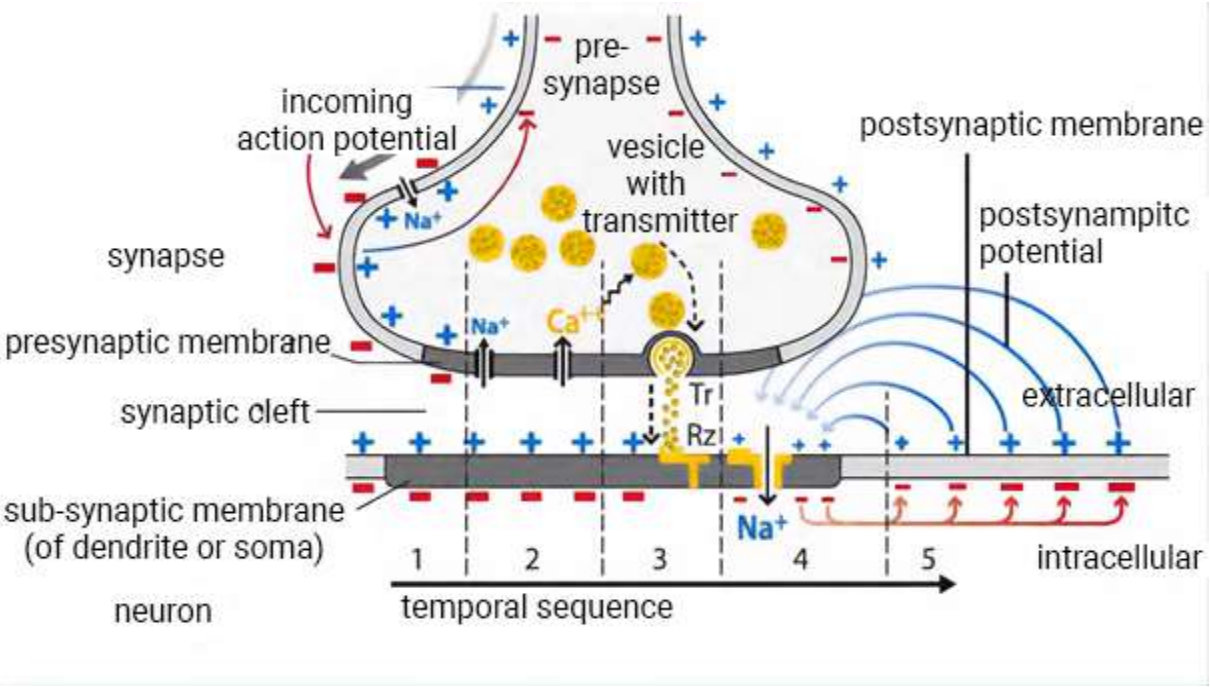

Figure 1-3 Schematic of the temporal course of the synaptic excitation. Modified after (Zschocke & Hansen, 2012) p. 3

them into the synaptic cleft when they reach the presynaptic membrane. The transmitter molecules diffuse through the approximately 20 nm large cleavage space and are then docking on to the receptors (Rz) of the subsynaptic membrane, resulting in a temporary opening of certain ion channels and pumps. This leads to an influx and efflux of ions specific to these channels, which ultimately changes the subsynaptic resting membrane potential.

Depending on which ion channels or pumps are opened by the chemical process of transmitter-receptor binding, a distinction is made between synapses that have an excitatory or an inhibitory effect. [12] Figure 1-3 shows excitatory transmission at an excitatory synapse. In the cerebrum, glutamate is the predominant transmitter molecule in this form of synapse [13]. Its binding to the receptors of the postsynaptic membrane results predominantly in the opening of Na^+ channels, which leads to a dominance of Na^+ influx. The result of this ion transport is a depolarization of the postsynaptic membrane by increasing the number of positive charge carriers on the inner side of the cell membrane, while decreasing them on its outer side. This implies an increase of the postsynaptic resting membrane potential, which ultimately favors the initiation of an action potential in the axon of the downstream neuron, thus the process has an overall excitatory effect.[14] The action of an

[11] (Thompson, 1994), p.94

[12] (Zschocke & Hansen, 2012), p.1

[13] (Zschocke & Hansen, 2012), p.4

[14] (Thompson, 1994), p.100-102

excitatory synapse causes the postsynaptic membrane of the downstream neuron to become less negatively charged, relative to the rest of the cell membrane.[13]

In an inhibitory synapse, the inverse effect to the excitatory synapse occurs. The released transmitter molecules, through their binding to the receptors of the postsynaptic membrane, predominantly cause the opening of K^+ pumps as well as Cl^- channels, whereas Na^+ channels remain closed.[15] This results in an outflow of K^+ ions from the cell interior (see Figure 1-4), as well as an influx of Cl^- ions into the intracellular region of the downstream neuron. Consequently, this leads to a negative shift in the resting membrane potential, which continues to the axon of the downstream neuron, making it more difficult to trigger an action potential in the downstream neuron, thus the overall effect on

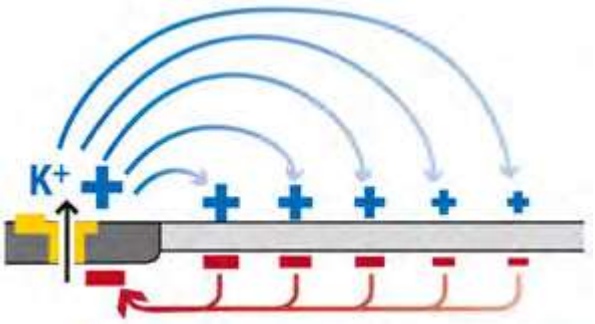

Figure 1-4 Schematics of a K+ ion channel. From (Zschocke & Hansen, 2012) p.3

excitation is inhibitory.[16] During this process, the outer side of the postsynaptic membrane becomes more positively charged due to the outflow of K+ ions from or the influx of Cl- ions into the cell interior, compared to the rest of the cell membrane of the downstream neuron.[16]

As is clear from Figure 1-3 and Figure 1-4 the local change in postsynaptic membrane potential induced in the synapse region leads to a change in the potential of the cell membrane sections adjacent to it. When the postsynaptic potential reaches the axon of the downstream neuron, there is an increase in the membrane potential in the case of excitatory postsynaptic potentials or a decrease in the membrane potential in the case of inhibitory postsynaptic potentials, which ultimately stimulates or inhibits the initiation of a new action potential according to the all-or-nothing law of excitation.

[15] (Thompson, 1994), p.104-105

[16] (Zschocke & Hansen, 2012), p.105

2 FORMATION PROCESS OF THE ELECTROENCEPHALOGRAM

After having shown elementary basics of neurophysics in section 1, the focus will now turn to the electrical processes in the cerebral cortex responsible for the electroencephalogram. In order not to overstretch the scope of this thesis and in order not to move too far away from biophysics towards biology, all considerations in section 2 are limited to the cortex unless explicitly stated otherwise. Due to this limitation, an explanation of the rhythmic structure of an EEG curve can only be dealt with superficially, since its cause is to be found in deeper brain regions and, moreover, this has not yet been fully clarified or is part of current research.[17]

2.1 CORTICAL FIELD POTENTIALS

Postsynaptic potentials cause charge carrier shifts in the clefts of the extracellular space. However, these shifts are not limited to the area immediately around the postsynaptic membrane, but spread over the neighboring brain volume, as shown schematically in Figure 2-1 for the movement of positive charge carriers due to the action of an excitatory postsynaptic potential.

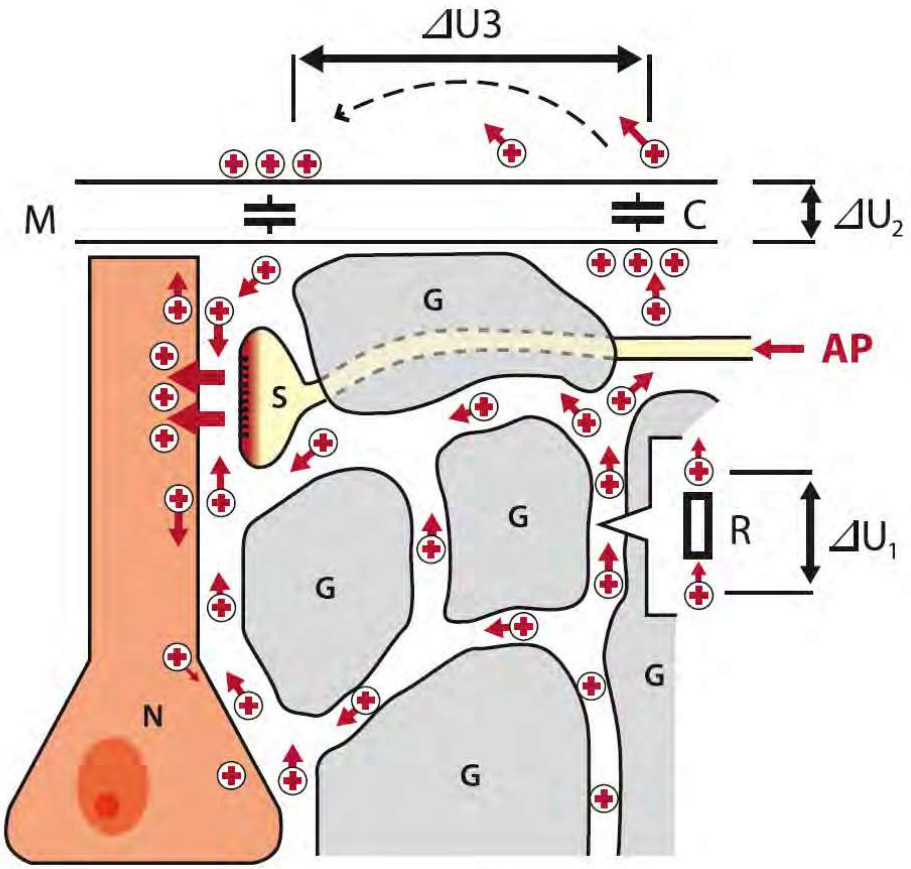

Figure 2-1 Movement of positive charge carriers due to the action of an excitatory postsynaptic potential. From (Zschocke & Hansen, 2012) p.7

[17] (Zschocke & Hansen, 2012), p.2

From a physical point of view, the charge carrier shift in the extracellular clefts is nothing other than an electric current. The cortical tissue, which can be thought of as a complexly interwoven network of ohmic resistors, induces a potential difference as current flows through it. Since electric current always prefers the path of least resistance and the tissue resistances have different magnitudes the ionic current spreads over a large area of the extracellular space. Starting from a single neuron, an entire area is created in the cortex tissue in which, by suitable conduction, electrical potential differences can be tapped, that are determined by the charge carrier shift triggered by synaptic excitation and the ohmic resistances of the brain tissue. The electric potentials of this field are called cortical field potentials.[18]

However, the ionic currents triggered by postsynaptic potentials in the brain do not reach the head surface where the EEG electrodes are placed, because between the brain and the head surface there are membrane or tissue structures (labeled M in Figure 2-1), such as meninges, the skull bone or the scalp, which have a very high DC resistance. These structures can be modeled like electrical capacitors, which can be charged and discharged differently by ionic currents in the brain or in other words, a voltage (such as ΔU2 in Figure 2-1) builds up between the fictitious capacitor plates. This ultimately ensures that cortical field potentials can propagate to the skull surface. These cortical field potentials, or more precisely the superposition of a multiplicity of cortical field potentials, each arising from a postsynaptic excitation, are now exactly those potentials which are measured by the electrodes of an EEG-device, as electrical potential difference between two points (ΔU3 in Figure 2-1) of the skull surface.[19]

In Figure 2-1, the letter G denotes the so-called glial cells. These cells are five times more abundant in the central nervous system than neurons and have, in addition to a tissue-stabilizing function, the task of controlling the transport of substances in the nervous tissue, in particular the regulation of the ion concentration in the extracellular space. From the previous considerations, it is not surprising that there is a contribution of glial cells in the process of formation of cortical potentials.[20] However, this process has not yet been completely clarified [19] and will therefore be neglected in the following considerations.

2.2 Cortical dipoles and field potential

All previous explanations of the causes of the potential differences registered in the electroencephalogram were of a purely membrane biophysical nature. Another modeling approach is to consider cortical field potentials as superposition potentials of electric dipoles, which form and change in time in brain tissue due to neuronal processes.[21] This, as will become clear in the following, makes the process of formation of the electroencephalogram clearer and easier to understand and certain aspects of the electroencephalogram even only become plausible through this dipole interpretation.

The exterior of the postsynaptic membrane of a neuron downstream of a synapse can be charged electrically more positively or more negatively with respect to the remaining regions of the cell membrane (i.e., the postsynaptic membrane) by synaptic excitation, depending on whether the

[18] (Zschocke & Hansen, 2012), p.6

[19] (Zschocke & Hansen, 2012), p.6-7

[20] (Zschocke & Hansen, 2012), p.14-17

[21] (Zschocke & Hansen, 2012), p.7-10

synapse is excitatory or inhibitory. Thus, from a physical point of view, an electrical negative pole is formed in an excitatory synapse, while the postsynaptic membrane sections of the neuron form a positive pole, thus overall an electrical dipole, the magnitude of which changes in time due to ion transport in the extracellular and intracellular areas. The same is true for an inhibitory synapse with a corresponding reversal of the signs. It should be noted that, contrary to the dipole definition of classical physics, these dipoles always point in the direction of the negative charge in the relevant literature. Postsynaptic potentials, therefore, can be considered as field potentials of electric dipoles, their field structure being influenced by the tissue surrounding the neuron. Since neurons have many synapses, each of which generates such a dipole when excited, the cortical field potential of a neuron is thus precisely the electric potential of the dipole resulting from the superposition of the individual postsynaptically excited (partial) dipoles of that neuron. However, the EEG electrodes do not record the dipole field of a single neuron, but the cortical field potential arising from the excitation of many cortex neurons. A direct consequence of this is that the stronger synaptic excitation processes occur synchronously at neighboring neurons in the cortex, the stronger the corresponding voltage deflection in the electroencephalogram, since the emerging dipoles of the single neurons occur simultaneously and thus the superposition potential can become particularly large in terms of magnitude.[22] It has been shown in animal experiments, among others, that the thalamus, which makes up a large part of the diencephalon and has a strong interconnection with the cortex, plays a central role for these synchronous excitations.[23]

The rhythmic activity of the smallest cell group areas, the specific thalamic nuclei, synchronizes the activity of cortical areas in the extent of square millimeters. During the formation of a group of waves, neighboring sites are included in the rhythm. In short, the thalamus is the pacemaker of synchronous electrical activity in the cortex. [24]

Since electric dipoles are vectors, not only the magnitude of cortical dipoles but also their direction is crucial for electroencephalography. This direction is determined by the spatial structure or geometry of the brain neurons.[25] Figure 2-2 shows the two main types of neurons occurring in the cerebral cortex: pyramidal and stellate cells. Pyramidal cells are neurons whose tip dendrites run vertically upward through the cortex before branching in the uppermost layer of the cortex. This shape creates

[22] (Zschocke & Hansen, 2012), p.7-8

[23] (Cooper, Osselton, & Shaw, 1984), p.7

[24] (Simon, 1977), p.5

[25] (Zschocke & Hansen, 2012), p.8

perpendicular dipoles in the cerebral cortex that are parallel to each other, with synchronized synaptic excitation of multiple pyramidal cells. They are the determining electrical dipoles for the

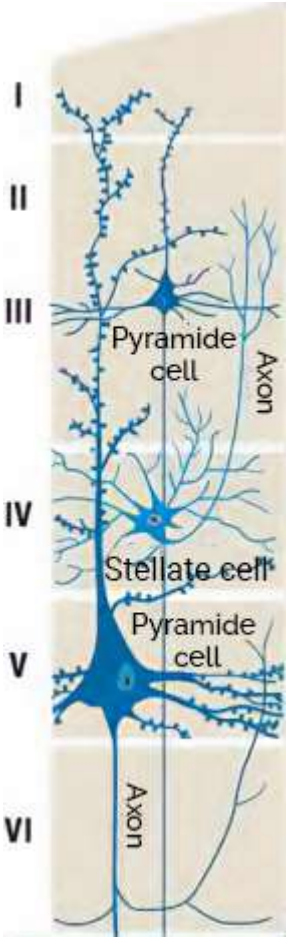

Figure 2-2 Form and placement of the pyramid and stellate cells in the six layers of the cortex. Modified after (Schmidt, Lang, & Heckmann, 2004) p. 189

potential fluctuations recorded in the electroencephalogram, although only about one third of the cortex neurons have such a spatial structure. [26]

[26] (Zschocke & Hansen, 2012), p. 8-9

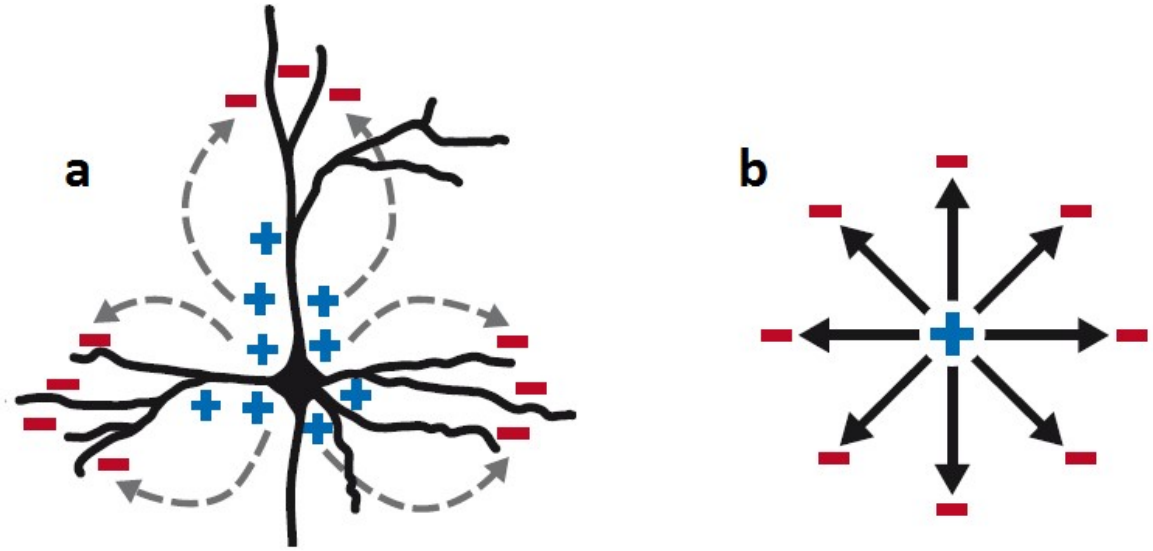

Figure 2-3 Dipole creation at the stellate cells. From (Zschocke & Hansen, 2012) p.8

Stellate cells, which make up most neurons, are switching neurons whose multiple dendrites run in different directions of the cortex. The single dipoles that form at each of these dendrites upon excitation therefore (nearly) cancel out in sum, as shown idealized in Figure 2-3 a and b, respectively. The dipole field of the stellate cells therefore has a rather less significant role on the electroencephalogram. [27]

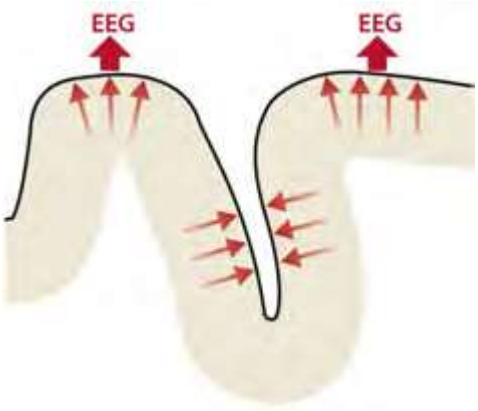

Figure 2-4 Cortical dipoles in the macrostructure of a brain furrow. From (Zschocke & Hansen, 2012) p.9

What has not been considered so far is the remote effect of cortical dipoles in the macroscopic structure of the cortex, which is furrowed. Since the EEG electrodes are placed on the skull surface, the electric field of those dipoles that form radially to it contributes the most to the final signal. On the other hand, the dipole fields formed in the cerebral grooves can be detected only partially because their field lines are tangential to the skull in the idealized case, i.e. the EEG electrodes are located on an equipotential surface of this electric field.[27] Cortical dipoles that form synchronously on

[27] (Zschocke & Hansen, 2012), p.9

opposite sides of a brain furrow (Figure 2-4) can influence each other reciprocally, which can lead to a cancellation of the dipoles.[28]

2.3 CORTICAL FIELD POTENTIALS AT THE CRANIAL SURFACE AND DC COMPONENT OF THE ELECTROENCEPHALOGRAM.

With the basic principles discussed so far, electroencephalography can now be defined as the recording of field potentials generated by electrical activity of neurons in the cerebral cortex. This recording with two electrodes each is performed directly on the scalp, i.e., potential differences of the projections of the electric dipole potentials onto the skull surface are measured. At this point it

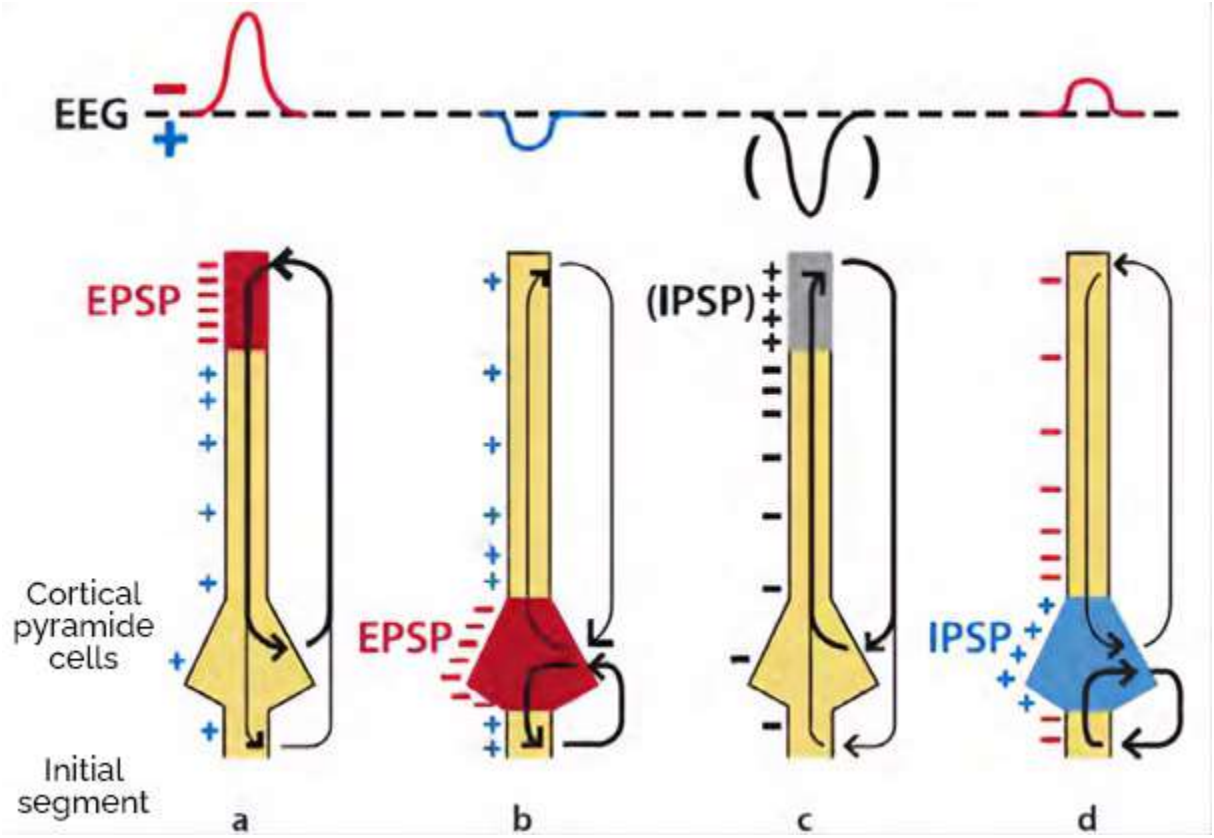

Figure 2-5 Cortical dipoles of a pyramid cell with the resulting polarity of the EEG signal. Modified after (Zschocke & Hansen, 2012) p.10

should be noted that in practice it is common to refer to the direction of deflection in the electroencephalogram as the polarity of the EEG signal. As illustrated in Figure 2-5 this depends on whether the synaptic excitation of the pyramidal cell membrane occurs at the soma or at the dendrites. Excitation at the dendrites is registered particularly strongly in the electroencephalogram because the resulting dipoles run close to the skull surface. Inhibitory postsynaptic potentials do not occur at the dendrites of the pyramidal cells of the outermost cortex layers, which results in the electroencephalogram being dominated by field potentials triggered by excitatory postsynaptic potentials at the dendrites of these cortex neurons.[28]

If a high number of excitatory postsynaptic potentials form in the cortex over a longer period, as is the case, for example, with sensory stimuli, it will come to a shift of the potential difference

[28] (Zschocke & Hansen, 2012), p.9-10

registered on the EEG device towards the negative, which can be detected particularly well by means of DC voltage amplification, as shown in Figure 2-6.[29]

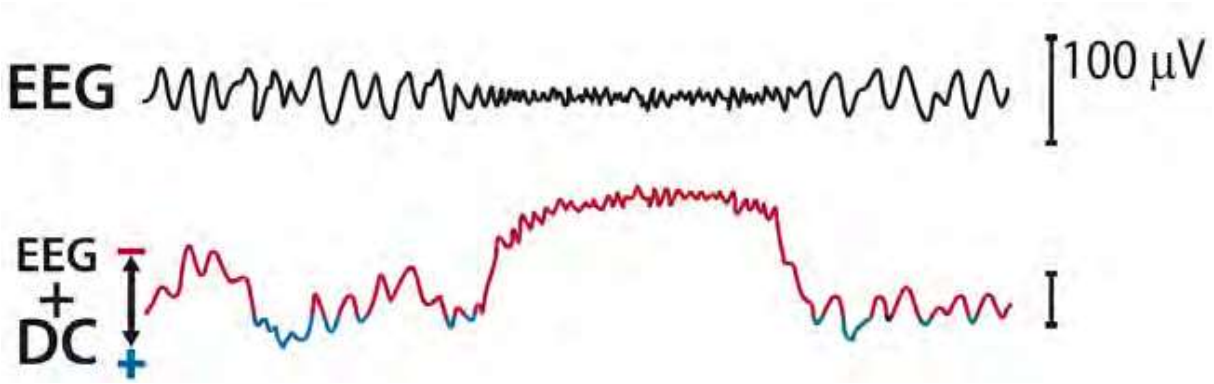

Figure 2-6 EEG signal with and without DC component. From (Zschocke & Hansen, 2012) p.12

It is obvious that this DC component of the electroencephalogram would be of importance for medical diagnostics in many cases. However, the DC component is superimposed by DC fluctuations of non-neuronal potential sources, such as the potentials of sweat glands in the skin, which are also registered by the EEG electrodes and whose amplitude is much higher compared to the cortical DC fluctuations. Especially these non-neuronal DC fluctuations would permanently overdrive the amplifiers in the EEG device, which is why they must be filtered out before the actual signal amplification. In this process, the DC voltage component, which is cortically conditioned, is also lost. What remains are the frequency-changing components of the tapped cortical potential difference in the µV range (Figure 2-6). This curve, additionally limited to a maximum frequency range of 30 Hz, is the raw EEG signal usually recorded in diagnostic practice.[29]

[29] (Zschocke & Hansen, 2012), p.13

3 MEASUREMENT OF THE ELECTROENCEPHALOGRAM

In this chapter I want to elaborate the measuring technology needed to record a viable electroencephalogram. The aim is to explain the basic characteristics and functions of the building blocks with a special emphasis placed on the input section of the EEG device, the amplifier technology, and the filtering process. I will not go into detail on how to build an EEG device as this will be the focus of the next chapter.

3.1 INFLUENCES OF ELECTRICAL RESISTANCES ON THE EEG MEASUREMENT

Figure 3-1 shows the highly simplified equivalent circuit of a single channel EEG device to a patient. The resistors shown here are to be thought of as impedances as we handle AC. The field potential difference reaching the skull surface is represented as a serial circuit of an AC voltage source U

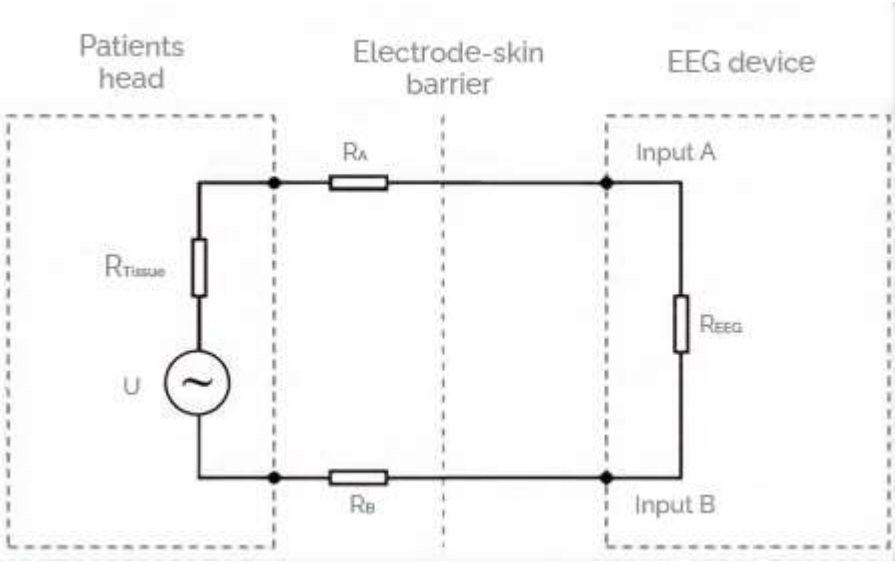

Figure 3-1 Simplified equivalent circuit of a single channel EEG device. From (Cooper, Osselton, & Shaw, 1984) p.52

(electrical potential difference of the cortex) and the tissue resistance R_{Tissue}. R_A and R_B are the two contact resistances at the connecting point between EEG electrode A and B on the scalp. The electrical resistances of the EEG device, especially those of the amplifier, are summarized as the internal resistance R_{EEG}.

Therefore, we can calculate the total resistance and the current flow as

$$R = R_{EEG} + R_{Tissue} + R_A + R_B$$

$$I = \frac{U}{R} = \frac{U}{R_{EEG} + R_{Tissue} + R_A + R_B}$$

To calculate the potential difference U_{EEG}, which is the relevant voltage for the EEG measurement we use:

$$U_{EEG} = I * R_{EEG} = \frac{U}{1 + \frac{R_{Tissue} + R_A + R_B}{R_{EEG}}}$$

This simplified look at the equivalent circuit diagram of the EEG measurement shows that the measured potential difference U_{EEG} is the actual voltage U lowered by a factor of $\frac{1}{1+\frac{R_{Tissue}+R_A+R_B}{R_{EEG}}}$. [30]

This factor implies that by increasing the internal resistance of the EEG device R_{EEG} and lowering the resistance between the electrodes and the scalp R_A and R_B the quality of the measurement can be improved drastically. The tissue resistance R_{Tissue} cannot not be influenced. The resistance values of the relevant tissue areas are listed in Table 1. [31]

Material	**Resistivity (Ωcm)**
Copper	$2 * 10^{-5}$
Seawater	20
CSF	64
Blood	150
Spinal cord (longitudinal)	180
Cortex (5 kHz)	230
Cortex (5 Hz)	350
White matter (average)	650
Spinal cord (transverse)	1200
Bone (100 Hz)	8000-16000
Pure water	$2*10^7$
Active membrane (squid axon)	$2*10^7$
Passive membrane (squid axon)	10^9

Table 1 Resistance values of relevant tissue areas

3.2 EEG AMPLIFIER

When the first EEG was measured by Hans Berger in 1929, he was using an extremely sensitive coil galvanometer.[32] Today a differential amplifier is commonly used as a feasible method to register a low interference amplified bioelectric signal in the microvolt range.[33]

3.2.1 Differential Amplifier

In a simple amplifier the signals of an electrode are measured or amplified against a zero potential, therefore any interference voltage is fully included in the amplified signal in addition to the

[30] (Cooper, Osselton, & Shaw, 1984), p. 52

[31] (Nunez & Srinivasan, 2006), p. 168

[32] (Kryger, Roth, & Dement, 2011), p.431

[33] (Zschocke & Hansen, 2012), p. 41

bioelectric signal. The most important interference voltage is the 50Hz voltage of the European power supply (in the U.S. this frequency is 60Hz). The inductively transmitted interference voltage will be discharged through the patient to the ground and is magnitudes higher than the bioelectrical fluctuations we can derive as EEG from the skull surface. Using a differential amplifier, we can measure two voltages against a zero potential and only amplify the difference between those signals. This leads to the suppression of a common interfering signal that is present in both voltage inputs. To what extent these common mode noise signals are suppressed is determined by the common mode suppression of the EEG amplifier. The disadvantage of using this in-phase signal suppression is that the EEG also contains in-phase signal components at the two points of measurement and these components increase the more the cerebral cortex activity is synchronized. These components are then treated as common mode signals and are not amplified. They remain masked in the EEG registration.

3.2.2 Common mode rejection

The suppression of same phase signals at the inputs of a differential amplifier is called common mode suppression. Unfortunately, a complete suppression of in-phase signals is technically impossible to realize as material deviations in the electronic components feeding to both inputs lead to deviations in the resulting in-phase signals.

More precise manufacturing of the electronic devices leads to better common-mode rejection. Its extent ("common-mode rejection ratio", CMRR) is therefore a quality characteristic of EEG amplifiers. The common-mode rejection ratio is defined by

$$\mathrm{CMRR} = \frac{\text{amplfication of out of phase signals}}{\text{amplfication of in} - \text{phase signals}}$$

The CMRR is particularly important for a viable EEG measurement as the amplitude levels of the brain waves are much smaller than interferences from surrounding electronic devices. The 50 Hz interference, for example, is many times higher than the level of the EEG signals under unfavorable ambient conditions, so that the common-mode rejection can then considerably reduce this in-phase interference signal but can no longer completely suppress it due to the above-mentioned tolerances of the components.

3.3 Filtering the EEG signal

Measured on the brains surface, the EEG contains signal frequencies between 0 (direct current) and approximately 100Hz. In clinical use the bandwidth is limited though using electronical filters. In the lower end of the spectrum slow potential fluctuations due to “sweating artefacts” and more commonly drifts of the electrode potentials are magnitudes higher then cerebral signals and therefore would overdrive the amplifier constantly. Therefore, signal below a threshold get filtered out despite losing the information that is caried by the slow-moving waves. [34]

On the higher end of the spectrum the distinct able EEG signals measured on the skulls surface tend to fade away above 30Hz. Therefore, a filter threshold of around 70Hz is used in clinical situations. This also leads to the suppression of high frequency interfering signals.[35]

[34] (Wellach, 2020), p. 31

[35] (Wellach, 2020), p.31

4 DESIGN DOCUMENTATION OF THE MODULAREEG

The aim of this thesis is to show that it is possible to build a working EEG device at home at a much lower cost than a medical grade machine and show the limitations of this device regarding measurement of brain activities. This thesis follows the guidelines published by the OpenEEG project.[36]

4.1 GENERAL REMARKS

For this project, the ModularEEG is used, which is a hardware solution developed in the OpenEEG project to capture EEG signals. The ModularEEG is a low-cost non-professional amplifier designed by Jörg Hansmann under the GNU General Public License.

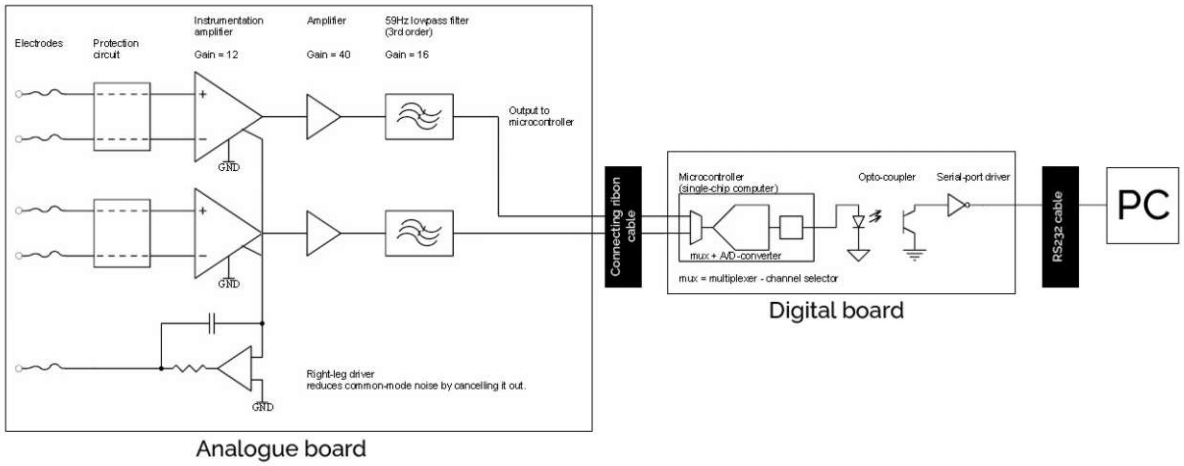

Figure 4-1 Block diagram of the ModularEEG. Modified after (OpenEEG design documentation, 2021).

The ModularEEG device consists at least of two separated boards: an analogue EEG amplifier which can serve two channels and a digital signal acquisition board to translate the analogue signals to digitals one. The ModularEEG design with the ATMega8 allows to operate 2 analogue boards one a single digital board which results in the maximum of 4 channels available for measurements.

Figure 4-1 shows a schematic overview over the complete design.

The general specifications for this device are as follows[37]:

Resolution	four 10 bits, two 8 bits
Input Voltage Resolution	0.5 uV
Input Voltage Full Scale	+/-256 uV
Wideband noise	~ 1 uVp-p
Supply Current (5V or 9 - 12V supply)	70 mA (2 channels)

[36] (OpenEEG Project page, 2021)

[37] (OpenEEG design documentation, 2021)

Isolation voltage	2500V (1 minute)
Continuous isolation voltage	480V

4.2 Operational overview

The EEG signal gets measured as the potential difference between two electrodes. Before entering the amplifying circuit, the signal is transmitted through a protective circuit that serves as a shield against electrostatic discharge (ESD) and protects the user of the EEG device against electrical voltages that may occur in case of a device failure.

The signal that is read by the electrodes on the scalp had an amplitude of only a few microvolts. Therefore, we must amplify it significantly before we are able to digitize it. Due to the small amplitude of the measured signal, interferences which are induced by the power grid (that is 50Hz in Europe and 60Hz in the US) are having a greatly negative influence in signal quality.

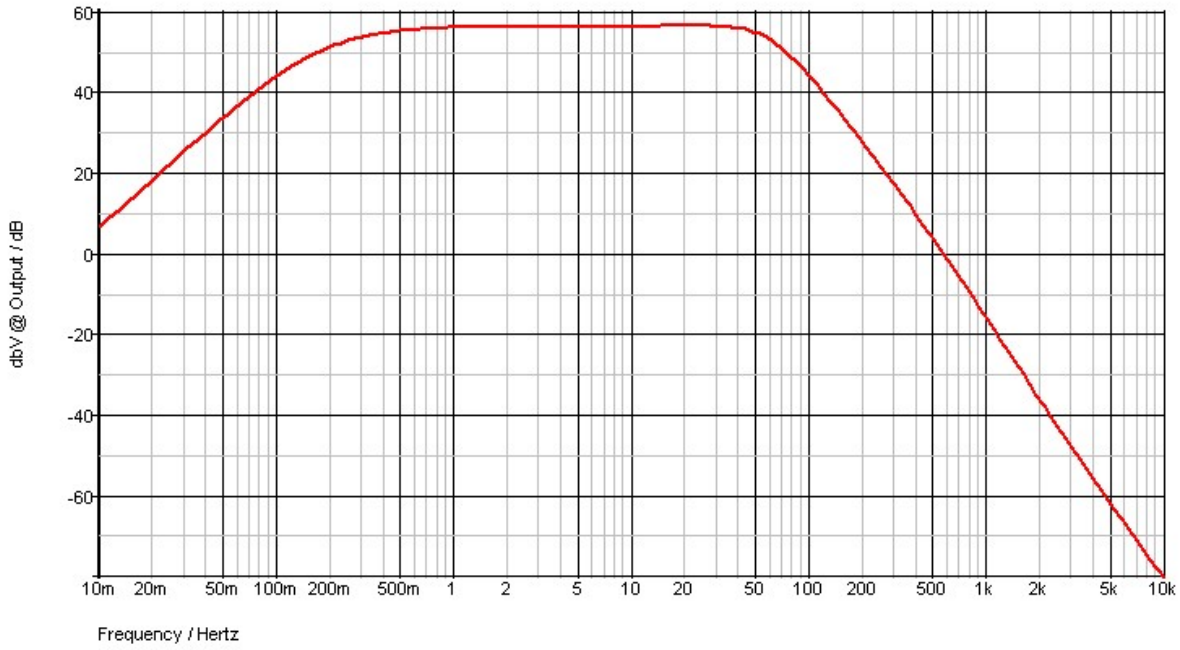

Figure 4-2 Filter gain profile of the ModularEEG. From (OpenEEG design documentation, 2021).

To solve this problem, the signal is first amplified with a high-quality differential amplifier that eliminates in phase signals from both electrodes and adds a gain factor of 12. This is followed by a high-pass filter that removes low-frequency oscillating signals (swimming) and then amplifies the result with an operational amplifier by a factor of 40. Finally, the signal is treated with an active low - pass filter having a gain of 16. The total signal gain before A/D conversion is therefore 7680.

Before the last amplification and filter stage, the signal is passed through the operational amplifier, back towards the user. This is the right-leg driver (RLD), whose purpose is to dampen network interference and the corresponding electrode should be sticked, as the name suggest, on the right light of the user. The RLD can reduce common mode signals up to 100 times more than the instrumentation amplifier by itself can do.

After filtering, the signal is ready for digitization. For this an ATMega8 microcontroller is used which provides the digitized signal that is then transmitted to a PC using a standard serial interface.

4.3 RS232 INTERFACE

The standard serial interface, which is shown in Figure 4-3, consists of three parts: the integrated circuit MAX232 (IC106), which converts RS232 voltage levels (usually ± 12 V) to TTL levels (0 V to 5 V) and vice versa. Two optical connectors (IC103 and IC104) electrically insulate the MAX232 from the rest of the circuit for safety purposes.

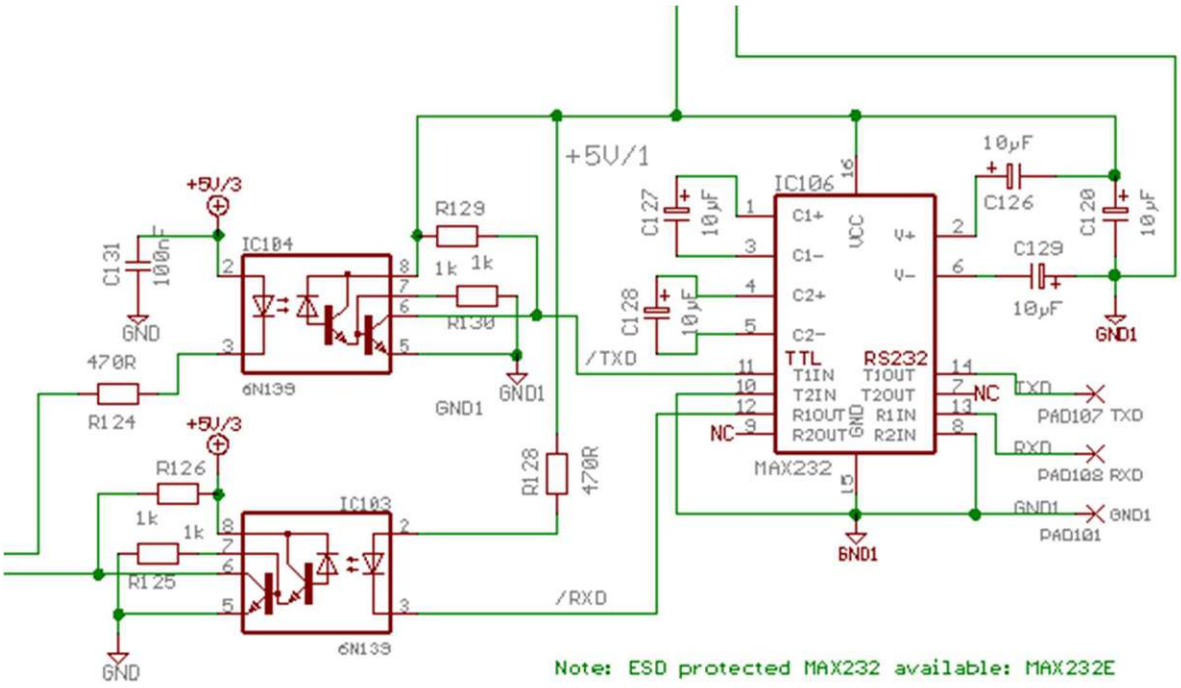

Figure 4-3 Standard serial interface consisting of an AD-converter and two optical connectors for insulation. From (ModularEEG digital board schematics, 2003)

4.4 AT90S4433/ATMEGA8 MICROCONTROLLER

The original design proposed by the OpenEEG project used the AT90S4433 microcontroller manufactured by Atmel. However, as this microcontroller is no longer being manufactured the ATmega8 turned out to be a good replacement as all the pins are compatible with the design of the AT90S4433 and the ATmega8 offers the same feature set. The only disadvantage of the ATmega8 over the AT90S4433 is that two of the 6 channels provided by the AD-converter are only 8 instead of 10 bits. This means that only 4 channels can be used for EEG measurements, while the remaining two can still be viable for measuring, for example, an ECG.

According to the design notes[38] the microcontroller was chosen for several reasons:

- Most instructions only take one clock cycle to execute.
- It has a built in 4-channel 10-bit AD-converter making it possible to measure 4 EEG signals at the same time, with two amplifier boards.
- It has a PWM-output which is used to generate a 14Hz square-wave signal. The signal is fed to the analog board where the amplitude is divided down to about 250uV, suitable for testing and trimming the EEG amplifiers.
- It has a full-duplex serial port.

[38] (OpenEEG design documentation, 2021)

- Programming is easy and does not require an expensive programmer.

The discrete parts next to the microcontroller are used primarily for creating a 4.0 V DC signal as a reference to the A/D converter.

The IC101 voltage regulator maintains a constant voltage, allowing for a controlled drop voltage across resistor R107. R107 (470 Ω) limits the current to about 2 mA, but its exact value determined by the voltage at input R of the voltage regulator IC101.

Resistors R102 and R103 form a voltage divider and a feedback path for the reference, so that at a cathode voltage of 4V, the input R of the voltage regulator sees 2.5V. If the input voltage is disturbed by a change in supply voltage, the reference will change the shunting current accordingly so that it will maintain 2.5 V at the input R of the voltage regulator.

Resistors R102 and R103 are connected in parallel to capacitor C101 with a capacitance of 10 µF, which is used as an energy accumulator, in the same way all other decoupling capacitors found in the circuit work. Diode D101 ensures that the reference voltage never exceeds supply voltage during switch-off.

R101 and R105 divides the 4.0V in two, creating an unbuffered 2.0 Volt reference for the VGND net. After that it is buffered on the analog board using an amplifier with gain of 1 commonly used to provide drive capability, which is the ability to force a signal to change, or to keep it at a desired level, by sinking or sourcing current into the wire. As the signal is constant in the ModularEEG the driving capabilities are not necessary here.

Finally, R111 and C108 (100 ohms + 10nF) provides extra High-frequency-rejection for the analog power input to the microcontroller.

4.5 POWER SUPPLY SYSTEM

The recommended way to power the ModularEEG is using a 9V or 12V battery. It is also possible to use a 5V external power supply as a second option but because the EEG is attached to the head a battery is the better option with regards to safety.

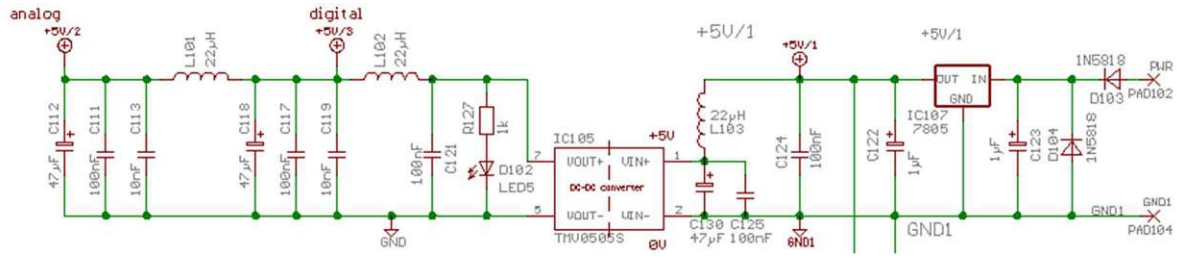

Figure 4-4 Schematic of the power supply circuit used on the digital board. From (ModularEEG digital board schematics, 2003)

A power source can be connected to the pads marked as PWR and GND1, which can be found on the top right corner of the schematic. If a battery with 9 or 12V is used, the diode D103 serves as a protection against damage from reverse polarity.

If a 5V source is used as a power supply, small modifications to the schematic need to be done: The diode D103 and voltage regulator IC107 are not used, and the pads need to be bridged using some wire. Also, the diode D104 is not needed when choosing an external power supply.

The output from the 7805 voltage-regulator is used to power two different parts of the circuit; the RS232 interface already described, and a DCDC converter (IC105). The DCDC converter acts an

isolation barrier that protects the user from high voltages while supplying power to the rest of the ModularEEG. It is designed to withstand continuous voltages of up to 1100 volts and spikes up to 3000 volts across its input and output.

The DCDC converter is followed by two filters. The purpose of those filters is to reduce the switching noise coming from the converter. The filter circuit is made up of two inductors L101 and L102 which utilize three capacitors each. Multiple capacitors are necessary as they can only work well withing a limited frequency band in real world conditions. While the 10nF capacitor handle the highest frequency components, the 47 uF capacitor is used to filter to the lowest frequency components. The power going to the microcontroller's digital part is filtered once, and the power going to the analog part and amplifiers is filtered twice.

The amplifiers on the analogue board need a dual power supply voltage, but the digital board only creates a single voltage. As described above a virtual ground VGND is created by feeding a 2V signal to an operational buffer amplifier on the analogue board (IC201A). This buffer then drives the virtual ground and therefore created a negative and a positive rail.

In short, what is used as GND on the digital board is renamed AGND and used as the negative power rail on the analog board. VGND = AGND + 2 volts acts as a virtual ground point for the amplifiers.

4.5.1 Summary

On the digital board, before isolation by the DCDC converter and throughout the RS232 interface we have the following currents:

PWR	incoming unisolated power
+5V/1	Unisolated, regulated 5V
GND1	Unisolated ground

The DCDC converter bridges the gap between unisolated and isolated and we have

+5V/3	Isolated 5V for the digital parts
+5V/2	Isolated and filtered 5V for the analog parts, including the amplifiers.
GND	Digital ground.

Finally, on the analog board we have

+5V/2	Analog power supply
VGND	Virtual ground, +2V referred to AGND
AGND	GND on the digital board

5 BUILDING THE EEG

The documentation of the OpenEEG project in general and the ModularEEG project specifically provides a wide variety of useful information on building the actual EEG. Also, the project is built to give the user a wide range of possibilities to achieve the wanted result.

5.1 ACQUIRING PARTS

5.1.1 Printed circuit boards

If the user is experienced in creating printed circuit boards, the necessary CAD files can be found in the projects sourceforge folder[39]. As the process of etching a PCB can be quite complicated and is prone to error the Bulgarian company Olimex[40] offers a great variety of possibilities for the inexperienced user. On their website either the empty printed circuit boards, analogue and digital, can be bought or even the prebuilt and configured ModularEEG is offered. For my thesis I bought the empty printed circuit boards for the digital and analogue parts of the EEG.

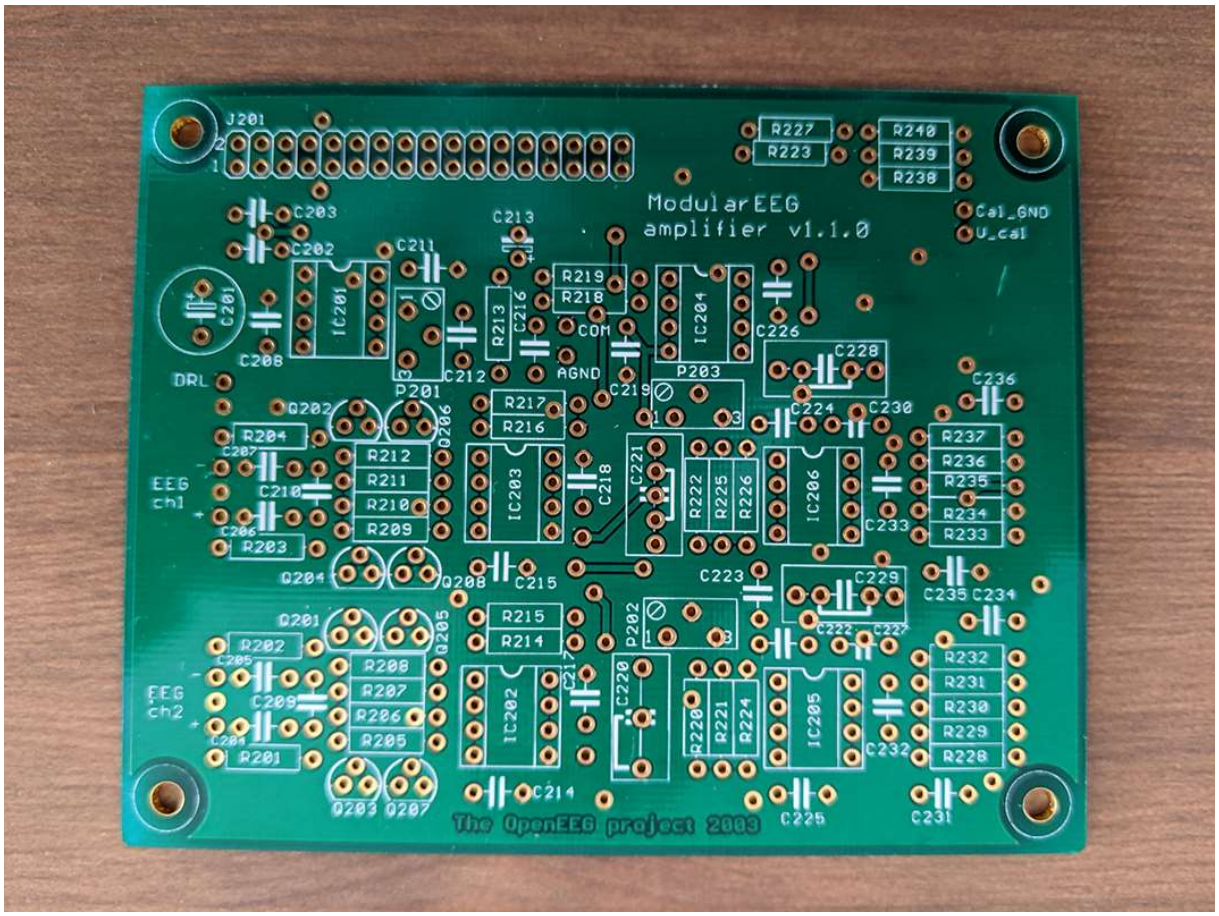

Figure 5-1 - Analogue amplifier PCB from Olimex

[39] (Sourceforge project OpenEEG, 2021)

[40] (Olimex OpenEEG, 2021)

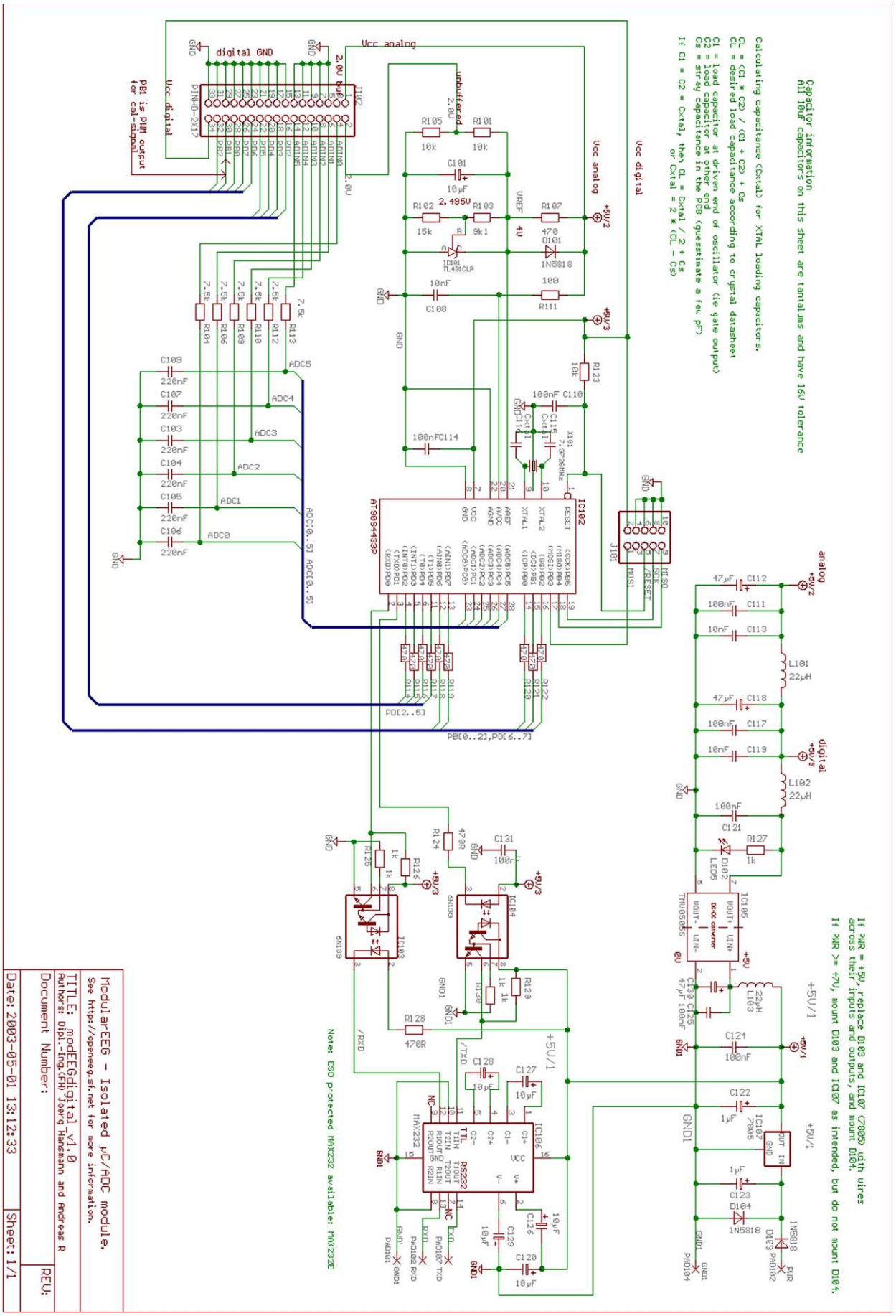

Figure 5-2 Complete schematics of the digital board used in the ModularEEG. From (ModularEEG digital board schematics, 2003)

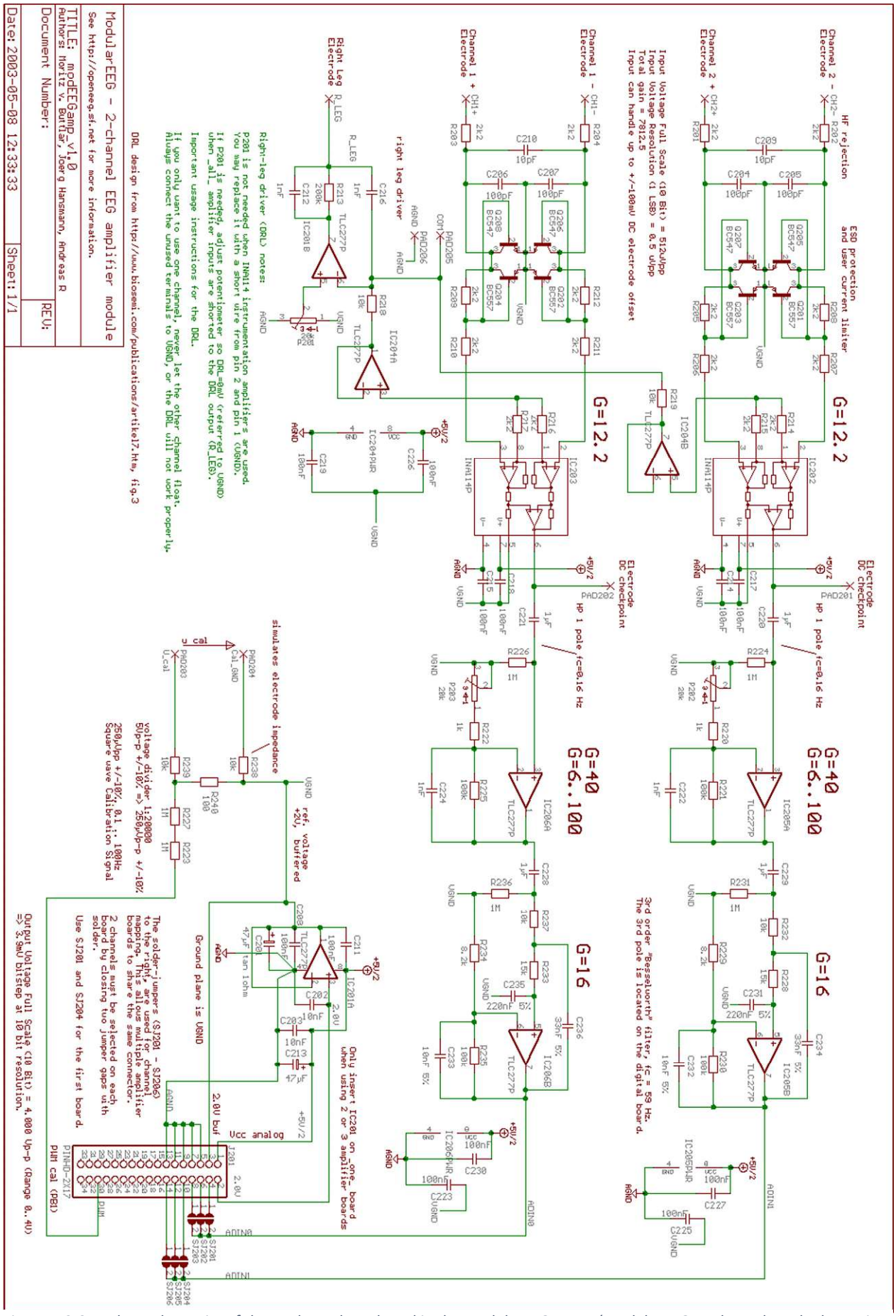

Figure 5-3 Complete schematics of the analogue board used in the ModularEEG. From (ModularEEG analogue board schematics, 2003)

5.1.2 Electrical components

In the most basic version, the ModularEEG consists of 45 parts that need to be soldered into the printed circuit board. The community of the OpenEEG project created a collective Excel Sheet where all required parts and the quantity for different configurations are listed. Also, the part-order-number for all parts are listed for four different electronics suppliers to make ordering the parts as easy as possible. [41]

The document provides a good overview of what is needed and gives a solid starting point for an ordering list but as it was last updated in 2003 it is quite outdated. Several components changed order-number or were no longer available at all. It took quite some time to find the correct substituting parts from several different electronics suppliers. I ended up buying from 4 different shops and spending more than necessary as parts often were not available in small quantities. This is to be kept in mind when trying to build an affordable EEG at home.

5.1.3 Cables

A few cables are needed to make the EEG work. First, I bought a serial cable which connects the EEG to the RS232 port of my PC. As RS232 ports are no longer a widely used standard, I had to buy a PCIe card to plug in to my computer that provides two RS232 interfaces. Also, a 3-pin connector and a small length of ribbon cable is needed to connect the PCB interface with the RS232 cable.

For programming the microcontroller using the built-in programming interface, a programming cable is needed. This can be made by the user (a document on how to do this is provided by OpenEEG[42]) or can also be bought from Olimex. I purchased the programming cable alongside the empty PCBs from Olimex.

Furthermore a 34-pin ribbon cable is needed to connect the digital and the analogue board as well as some copper wire for connecting the electrode inputs to the PCB pads.

5.1.4 Casing

The analogue board needs to be shielded in a metal case to filter out signal noise that would render the measurement of the small amplitudes produced by electrodes impossible. Those cases can be bought in almost any electronics store but are much more expensive than I would have thought. Therefore, I opted for an old aluminum cookie box I had at home which coincidentally had the perfect size to fit the PCB and the plugs for the electrodes.

5.1.5 Electrodes

The electrodes are one of the most delicate parts of the project. They need to be made from a well conducting material and the cables need to be very well shielded to not pick up too much noise. I used a solid microphone cable and two smaller cables with banana plugs on the end. Also, I bought one-time-use electrode pads intended to be used in combination with an ECG and connector pins that can be plugged into the banana plugs.

To easily connect the electrodes to the EEG device I used 3.5mm phone connectors. The male parts were soldered on the end of the electrodes cable while the female part is screwed into the EEG casing and is connected to the PCB on the inside.

---

[41] (Sourceforge project OpenEEG, 2021)

[42] (ModularEEG Building instructions, 2021)

5.2 Assembling the EEG

After purchasing all needed components, the assemblance of the EEG can be done. First the electrical parts are soldered on to the two printed circuit boards, the digital and the analogue one. After that the electrodes are soldered, and the casing is prepared with the female phone connectors. The final step is to place the boards into the casing and connect all necessary cables.

5.2.1 Assembling the boards

The pads on the PCB are marked with the code for the electrical component that should be placed there. To make life easier it is best to first start with the components that have the lowest height profile so you can turn the PCB over and rest it on the tabletop without the components falling out of it again. The recommended order by the OpenEEG project is:

1. Small diodes
2. Resistors
3. The microcontroller crystal
4. Large diodes
5. Inductors
6. IC sockets
7. Socket strips, if used.
8. The 7805 voltage regulator
9. Ceramic capacitors
10. The transistors and the voltage reference.
11. Electrolytic capacitors
12. Film capacitors
13. Trim potentiometers
14. Ribbon cable connectors (pin headers)
15. The DCDC converter

Also, the ICs should remain in their anti-static packing until they are used as they are extremely sensitive to static discharge. After soldering every component to the correct spots on the PCB make sure that the legs are trimmed, and no connection is made where it should not be. Finally, the channel selection soldering pads on the back of the analogue amplifier board need to be bridged according to the number of amplifier boards you have. The final boards can be seen in Figure 5-4.

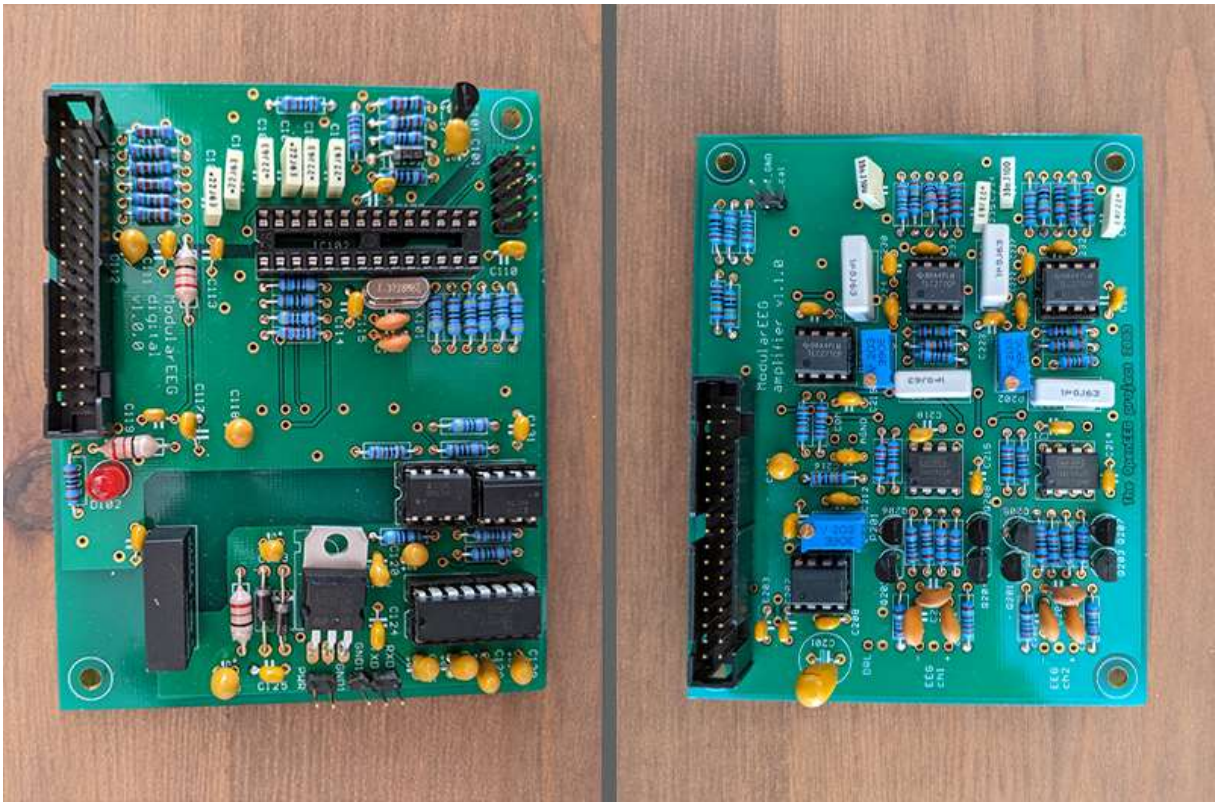

Figure 5-4 – Fully equipped digital and analogue board. Only the ATMega8 microcontroller is still missing on the digital board.

5.2.2 Testing the digital board

Before connecting the digital board to the amplifier board and installing the microcontroller, it should be tested if the basic voltages are correct following these steps:

1. Before powering up, ensure using an ohmmeter that there is no short circuit between GND1 and +5V/1 network or GND and the +5V/2 net.
2. Connect to your power source and turn on the power. The LED should light up.
3. Ensure that the voltage between L103 and GND1 is 5V
4. Ensure that the voltage between L102 and GND is somewhere between 5V and 5.5V

5.2.3 Making the programming cable

The OpenEEG project offers instructions on how to make your own programming cable for those who are interested in that or want to keep their budget small. The schematic can be found in Figure 5-5.

For this thesis I bought a programming cable from Olimex. [43]

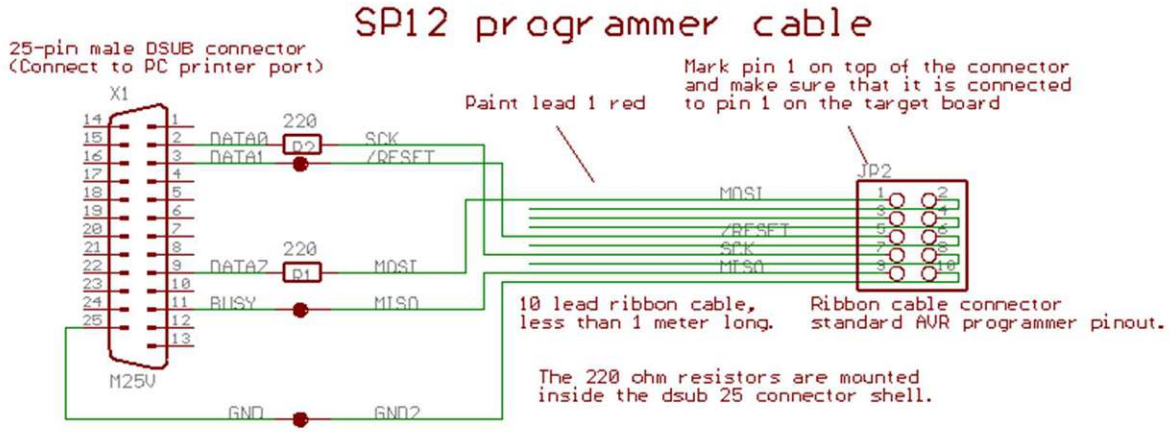

Figure 5-5 Schematic of the microcontroller programming cable as proposed by the OpenEEG project. From (ModularEEG Building instructions, 2021)

5.2.4 Programming the Microcontroller

The microcontroller on the digital board can be programmed using the programming cable that connects the programming interface to your PC. The ModularEEG project provides a firmware and installation instructions for the ATMega8 as well as for the AT90S4433. The software recommended by the authors of the firmware to program the microcontroller can run under Windows XP or older. I was not able to get results using it on Windows 10. Therefore, I switched to using a Linux setup and installed the software "SP12". Then going through the following steps, I was able to program the ATMega8 microcontroller:

1. Open the shell and go to the directory where the SP12 software is kept.
2. The first time running the program after the installation the command "*sp12 -i*" needs to be run, which allows sp12 to initialize itself.
3. Connect the EEG to the PC using the programming cable.
4. When using the ATMega8 controller the fuses need to be set as a first step by running the command
    - *"sp12 -wF11111111"*
5. Finally program the ModularEEG with the following command assuming the latest firmware for the ATMega8 is used
    - *"sp12 -wpf atmega8_modeeg-p2.hex "*

After that, disconnect the EEG from the PC again. The microcontroller is now programmed.

5.2.5 Making the RS232 cable

For connecting the EEG to the PC, a RS232 interface is used. For this thesis I used a 4-pin cable connector with an attached female RS232 head that I already had at home. To elongate the cable, I used two RS232 connector pinheads and soldered them at the ends of a three-pole-cable. To make communication between the EEG and the PC possible without a modem in the middle, the pins 1 (DCD), 4 (DTR) and 6 (DSR) had to be connected.

[43] (Olimex OpenEEG, 2021)

5.2.6 Testing the microcontroller

For testing the microcontroller, we need to first install the software “ElectricGuru” and connect the EEG to the PC using the RS232 cable. Next power up the EEG and follow these steps:

1. Run ElectricGuru and open the preferences menu.
2. Select the “Serial Port” menu item and select the right serial port in the dialog
3. Select the "Machine" menu item and choose "RS232EEG" in the dialog.
4. Finally select the "Traces" menu item and change the following settings in the dialog: The Y-axis limits should be 0 and 1023. "Show which samples" should be set to "All".
5. Start ElectricGuru by clicking the green stoplight button.
6. You should see two flat-line traces being drawn.

5.2.7 Testing and trimming the analogue board

5.2.7.1 A first test

First let’s check if the combination of analogue and digital board is working correctly and connect it to the PC.

1. Verify again that there are no short circuits between the positive power rail, VGND and the negative power rail.
2. Insert the amplifying integrated circuits and connect the analogue board to the digital board.
3. Connect the ModularEEG to the computer via RS232 and run ElectricGuru.
4. Connect the EEG to the power source.
5. Start ElectricGuru by clicking the green stoplight button – a lot of main hum from the electric power grid should appear.

5.2.7.2 Coarse trimming

To calibrate the signals using the trimmer potentiometers, the ModularEEG design provides an output U_cal and a calibration ground Cal_GND. Using the square wave signal that can be measured between those two reference points the trimming potentiometer can be utilized to calibrate the amplitude of the input signal. The calibration process needs to be done for each channel.

1. The ModularEEG must be powered down.
2. The calibration signal needs to be fed into the input of one EEG channel by connecting U_cal and Cal_GND to the channels input.
3. After starting ElectricGuru with the green stoplight button a square wave should be drawn on one channel.
4. Depending on the chosen channel the trimming potentiometer P202 or P203 needs to be adjusted using a small, flat screwdriver until the square wave is slightly less than half scale.
5. The traces dialog needs to be opened from the preferences menu.
6. After adjusting the window height so that the traces become as large as possible the y-axis limits need to be set to 262 and 762.
7. Finally, after closing the dialog and the gain needs to be adjusted with the trimming potentiometer until the square wave just touches the top and bottom of the graph window.

5.2.8 Fine trimming

Note: In theory the test signal should have an amplitude of 250uV peak to peak. This would lead to a square wave signal alternating between the values 262 and 762 when sampled. However, under real life conditions the signal amplitude depends on the supply voltage U, which should be 5V but will never be precisely of that value. Therefore, the actual amplitude of the square wave becomes U/20000 volts peak to peak. To compensate for that our upper bound in sample values will be

calculated as M+U*50 and our lower bound as M-U*50, where M is the average sample value. To get the square wave to be exactly between those bounds, the following steps need to be executed:

1. The supply voltage U needs to be determined by measuring the potential difference between any point on the +5V/3 net and GND.
2. In the traces dialog the Ymin and Ymax value need to be adjusted until the square wave signal is visible and centered in the graph window
3. M is to be calculated using the Ymin and Ymax value and M=(YMin+Ymax)/2
4. In the traces dialog Ymin should be set to the lower bound value calculated by M-U*50 and Ymax should represent the upper bound value M+U*50. With an ideal supply voltage of 5V these values should turn out to be 262 and 762 respectively but as mentioned above they differ in real world conditions.
5. Now the square wave needs to be adjusted using the trimming potentiometer until it is reaching the bound represented by the traces graph.

With those steps the trimming of the channel is completed.

5.2.9 Putting the boards into the casing

After the boards are assembled and calibrated, they need to be put into a casing. The OpenEEG guidelines recommend putting the analogue board into a metal container, that acts as a shield and then put this metal box and the digital board inside a plastic enclosure.

Figure 5-6 – The analogue board inside the casing. The female 3.5mm phone jacks can be seen at the top and the left of the image. Note that the two left inputs are not connected in the top row as they are a leftover from a previous design.

I chose a different approach and did not use a plastic casing. Instead, I screwed the analogue board inside a metal cookie box. For this I used plastic spacers so that the PCB is not connected to the casing (see Figure 5-6). The digital board was screwed on top of the lid using the same plastic spacers. The ribbon cable that connects the digital and analogue board is lead through the gap that the lid provides.

To give easy access to the electrodes the female counterpart of the 3.5mm phone jacks were mounted on the side of the casing and are connected to the analogue board inside. (See Figure 5-7)

Figure 5-7 – Left: Input connectors for electrodes. The existence of 4 plugs is a relict of an earlier design trial. Only the two ports marked as CH1 are active and each of them is used to plug in one channel. Right: Input for the DRL electrode.

5.2.10 Making the electrodes

The electrodes for the EEG are a crucial part of the whole system. They need to pick up the extremely small signals on the scalp and make sure that they do not get drowned in electric noise while transmission. There are two kinds of electrodes to choose from.

5.2.10.1 Passive electrodes

Passive electrodes have no inbuilt circuit. They consist of a metal pad and a shielded cable that transmits the signal from the head to the EEG device. A saline gel is needed to ensure good contact with the skin.

5.2.10.2 Active electrodes

Active electrodes are just like passive electrodes metal pads and a shielded cable but have an additional amplifying circuit built in. This amplifies the signal directly on the scalp which neglects noise from the cables and gives a better signal quality. Also, no conductive paste is needed using active electrodes.

Although there are some designs for building active electrodes available on the OpenEEG page I decided to go with passive ones for this thesis as the active electrodes would need further investigation and this thesis should be more a proof of concept.

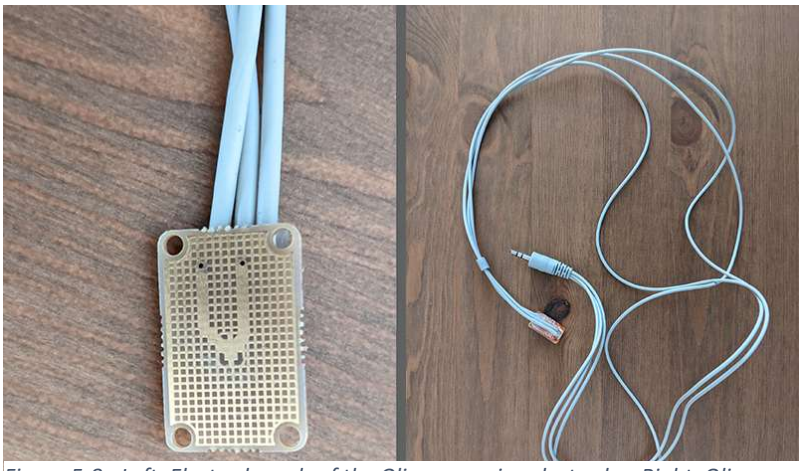

Figure 5-8 - Left: Electrode pads of the Olimex passive electrodes. Right: Olimex passive electrodes

For this thesis multiple tries were necessary to figure out the best way to build the electrodes. As a first try I bought some electrodes from Olimex, which come already prepared with a 3.5 mm phone connector. The electrodes are made of a small piece of plastic with small metal pads on one side. (see Figure 5-8) After connecting the electrodes to the EEG only noise signal was to be detected. I tried using a saline solution of about 1% concentration and putting it on the pads, but the result was not improved. Even after using a store-bought electrode gel only noise was visible in the signal. As the cables of the electrodes are very thin, I assume they are just not sufficiently shielded to ensure a good signal quality.

To improve signal quality, I replaced the thin cables on the Olimex electrodes with a well shielded microphone cable and attached a 3.5mm phone connector to it. The shield wiring of the cable was passed through the phone connector and fed into the GND of the analogue board. Using this setup, I was able to get first hints of a meaningful signal but still the noise level was too high to have real use.

Figure 5-9 – Left: Silver-chloride patch of the electrodes visible in the center. Right: Connecting pin for measurements on the back of the electrodes

Also, I had troubles keeping the electrodes close to my skin as they are not adhesive and in combination with a conductive gel can be very slippery.

As a last step in improving the electrodes I ended up using professional electrode pads, which are self-adhesive and have a connecting pin on the backside. They use silver-chloride as an electrode which is surrounded by conducting tissue (see Figure 5-9). I then removed the Olimex electrodes from the microphone cable and replaced them with connectors that would fit the back of the electrode pads. The design also involves using the same shielded cable for the two electrodes used in the same channel. The two electrodes are connecting to the microphone cable using a thinner, more flexible wire with banana plugs on the end. To minimize the distance of unshielded cable while giving the necessary freedom of movement to place the electrodes, the banana plug cables are only about 10cm long. The final design can be seen in Figure 5-10.

Figure 5-10- The final electrode design using a shielded microphone cable, a 3.5mm phone connector and two banana plugs ending in a connecting plug for the electrode pads

Using this setup, I was able to get good contact and a meaningful signal quality from the electrodes.

6 TESTING THE EEG

The EEG device I built during this thesis has some limitations when compared to a medical grade one. The numbers of input-channels are limited to two which makes the typical use of the 10-20 system

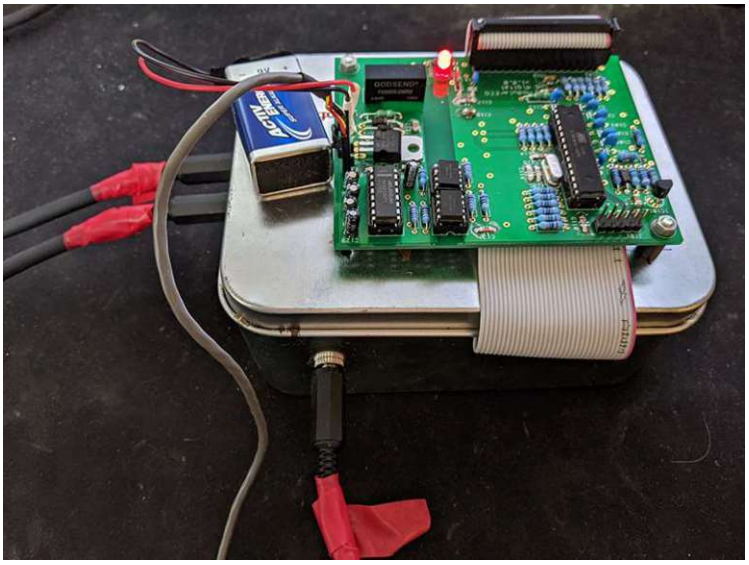

Figure 6-1- The complete setup for EEG measurements. On the left the two cables going to the channel electrodes can be seen. In front the input for the DRL is shown. The board seen on top of the casing is the digital board powered by a 9V battery.

with its needed 21 electrodes not possible. Also, the self-adhesive electrode pads need skin contact

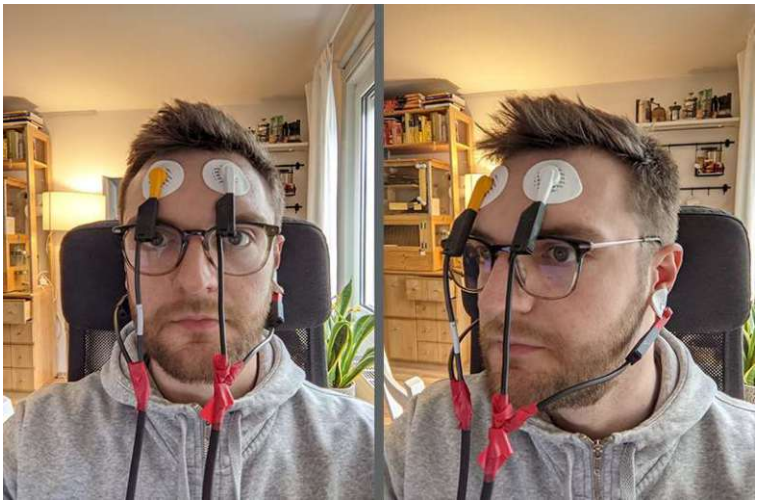

Figure 6-2 Electrode placement according to the 10- 20 system. Fp1 and Fp2 are used and A1 and A2 are the corresponding reference points.

to work as no external mechanism is holding the electrodes. Therefore, measurements on the parts of the scalp that have hair cannot be done. Due to this limitation I decided to take measurements only using the measuring points on the forehead Fp1 and Fp2 with reference to the earlobes A1 and A2, respectively as seen in Figure 6-2.

6.1 METHODS OF FILTERING THE MAIN HUM

Interference from noise produced by electrical power lines is one of the biggest challenges when recording biosignals which have an exceedingly small amplitude and therefore can be significantly disturbed by the electromagnetic interference that is induced in the human body. Power supply artifact effects have been modeled through the equation described by Huhta and Webster consisting of the magnetic induction, the displacement current in leads, the displacement currents in the human body, the common mode gain, and the effect of electrode impedances.[44]

There are two general ways to dampen the amount of main hum in the signal: software-based filtering and hardware-based filtering. The software approach is to apply a digital filter to a recorded signal with noise in it, while the hardware approach aims to suppress the recording of the noise in the first place.

6.1.1 Driven right leg circuit

The concept behind the DRL is to drive the potential of the body with the inverted common-mode signal obtained by the measurement to cancel out the inducted main hum[45]. The name stems from the fact that the electrode used for the DRL is placed at the end of the right leg to be the furthest away from the desired measurement point. The power-line noise usually is not a pure 60 or 50Hz sinusoid wave but is distorted with artefacts. Therefore, one major advantage of using a DRL circuit for attenuating main hum is that the common-mode signal recorded by the right leg electrode, is truly correlated with the noise in the EEG recording. This allows for a more precise elimination of power line signals. [46]

6.1.2 Digital filtering

When it comes to digital signal filtering there are two major categories that digital filter algorithms can be divided into: finite impulse reaction (FIR) filter and infinite impulse reaction (IIR) filters. [47] The main difference between those two is that FIR filters work by multiplying the data points with a relatively long filter kernel while IIR filters use a feedback loop of the already filtered data in addition to the truly short filter kernel. [48]One major advantage of IIR filters over FIR filters is the faster calculation speed with the biggest disadvantage being the possible instability of the filtered signal. As the processing of the signals for this thesis is not speed relevant, I chose to go with a FIR filter design as described by Parks and Burrus[49] for all further experiments.

6.2 COMPARING DRL AND DIGITAL FILTER QUALITY WITH RAW SIGNAL

6.2.1 Unfiltered signal

In Figure 6-4 a recorded EEG signal is shown while the user was at rest. The signal is completely obscured by the main hum noise and no significant structure in the signal can be seen. This is confirmed by calculating the corresponding power spectrum shown in Figure 6-3. Here it can be

---

[44] (Huhta & Webster, 1973)

[45] (Wong, Pun, Zhang, & Choy, 2006)

[46] (Thakor & Zhu, 1991)

[47] (Vaseghi, 2008)

[48] (Smith, 1997)

[49] (Parks & Burrus, 1987)

obtained that the induced amplitude of the power line noise a approximately about a factor of ten higher than any other frequency of interest.

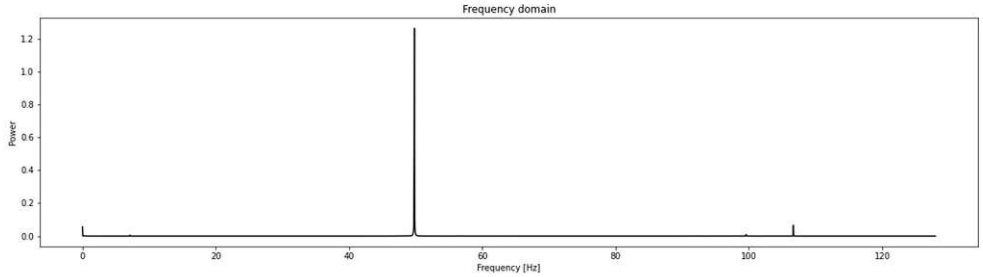

Figure 6-3 FFT analysis of the recorded signal of the user's brain in rest without any method of filtering the main hum. The power spectrum clearly shows the main hum drowning every other frequency by a factor of approximately ten

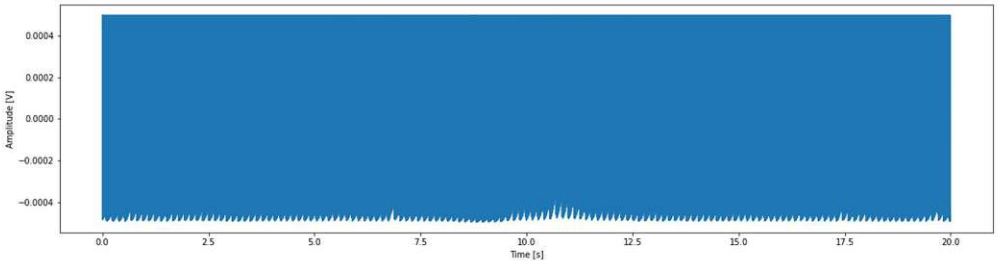

Figure 6-4 Recorded signal of the user's brain in rest without any method of filtering the main hum. The 50Hz frequency is too dominant to see any significant data.

6.2.2 Using a digital filter

Applying a digital FIR notch filter to the same signal recorded without a DRL electrode attached to the body improved the signal significantly. The filter method was MatLabs firls and the used filter

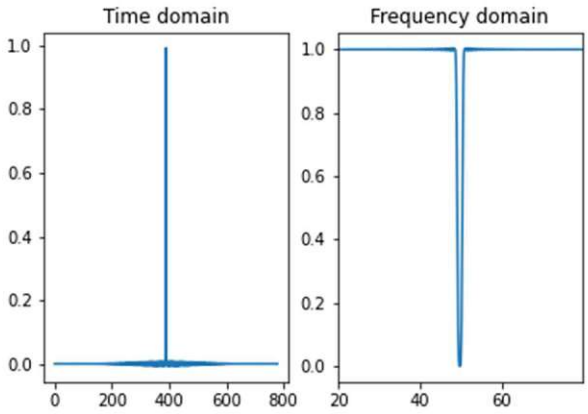

Figure 6-5 The generated time and frequency domain of the 50Hz notch filter kernel used to filter out the power line noise.

kernel can be seen in Figure 6-5. The filtered signal and the corresponding power spectrum can be seen in Figure 6-6 and Figure 6-7 respectively. The 50 Hz main hum was almost completely

attenuated and the time domain of the signal revealed artefacts from blinking (e.g. at around second 7 of the recording) that were masked before.

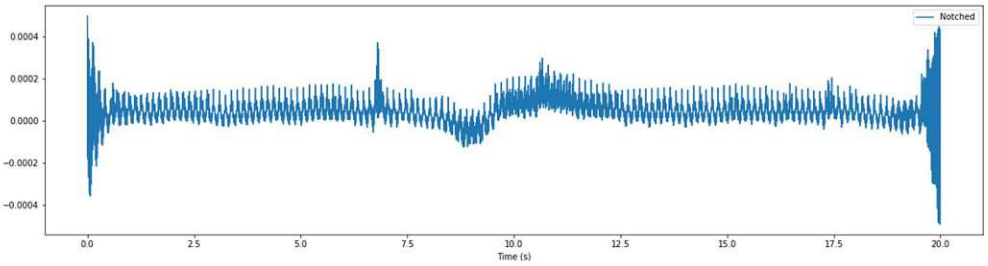

Figure 6-6 EEG signal of the user's brain in rest without a DRL but with a digital notch 50Hz notch filter applied. The signal improvement is significant and even reveals artifacts in the recording, for example a signal spike at around 7 seconds when the user blinked.

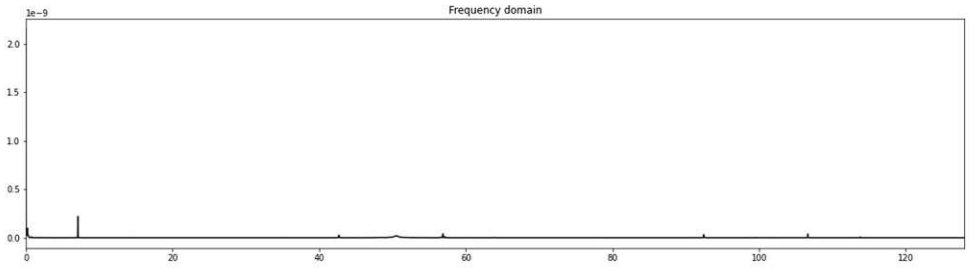

Figure 6-7 Power spectrum of the EEG signal recorded without DRL in rest with an applied digital filter to it. The main hum at 50 Hz is no longer present.

6.2.3 Using a DRL as a mean of filtering common-mode signals

As discussed before using a driven right leg circuit to drive the body's potential is another viable approach for filtering common mode signals and therefore attenuating power line noise. Again the user was sitting at rest when attached to the EEG. The DRL electrode was attached to the right leg, just above the ankle. The resulting time domain of the signal is shown in Figure 6-8.The signal is still dominated by the power line interferences but certain spikes when the user blinked are visible, where without a DRL this was not possible to identify.

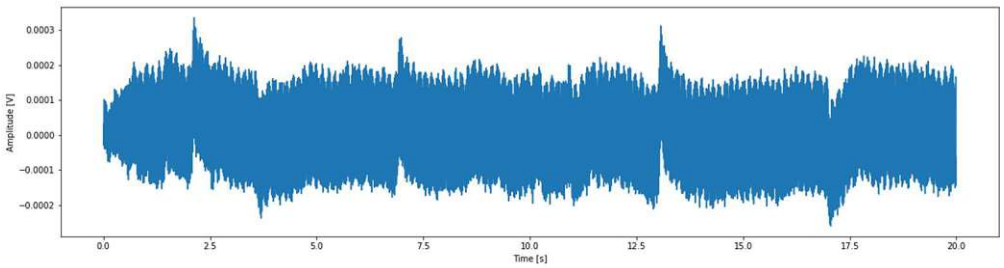

Figure 6-8 Recorded signal of the user's brain in rest with an attached driven right leg circuit.

As shown in Figure 6-9, the amplitude of the 50Hz frequencies in the power spectrum is reduced by a factor of 6 when compared to the recording without a DRL. However, this is still much higher than the signal of interest.

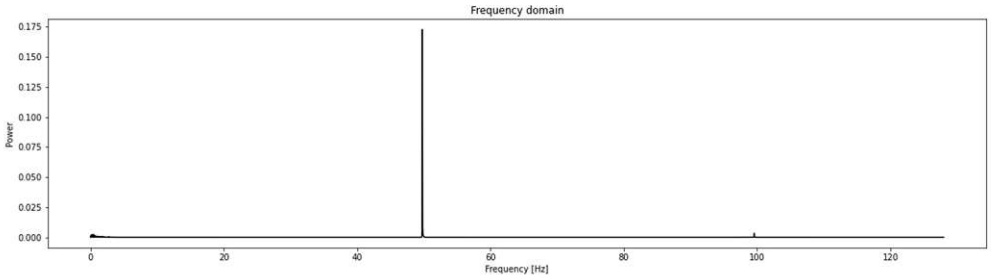

Figure 6-9 Power spectrum of the EEG signal recorded with DRL in rest. The amplitude of the 50 Hz main hum is reduced by a factor of 6 compared to the signal obtained without using a DRL.

6.2.4 Combining DRL and digital signal filtering

The DRL alone was not able to suppress the power line interferences completely but nevertheless provided a significant improvement in the signal quality. When applying a digital filter to the already improved signal obtained with an attached DRL a further attenuation of the unwanted interferences can be expected. The result of using a 50Hz notch filter on the signal shown in Figure 6-8 can be seen in Figure 6-10. The signal quality improved drastically as the main hum is attenuated effectively. This is also shown in the FFT analysis seen in Figure 6-11.

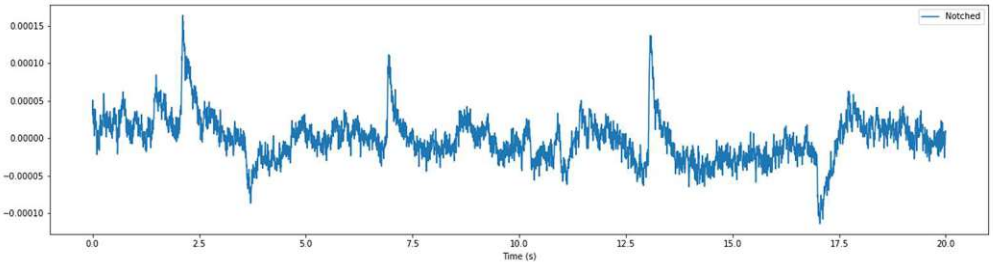

Figure 6-10 Recorded signal of the user's brain in rest with an attached driven right leg circuit and an additional 50Hz notch filter digitally applied to it.

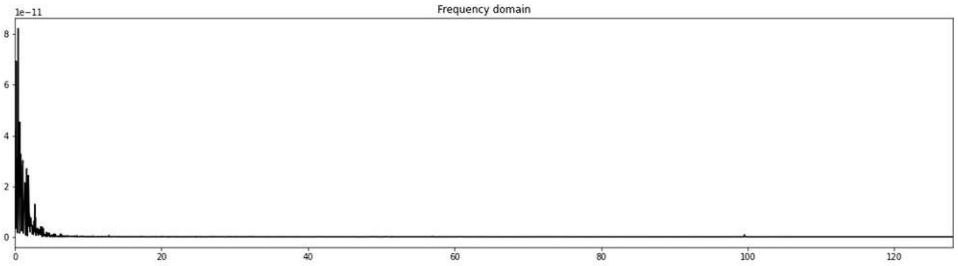

Figure 6-11 Power spectrum of the user's brain in rest with an attached driven right leg circuit and an additional 50Hz notch filter digitally applied to it. Main hum is suppressed completely.

6.3 EYE MOVEMENT

Artifacts caused by the movement of the eyes are the most frequent of all biological artifacts[50] and are also mostly unavoidable. In the eye, dipole-like structures are also formed between the cornea and the retina. The cornea is positively charged with respect to the retina and the potential difference between them is about 100 mV. Both blinking and movement of the eyeball itself change the electric field of this dipole structure.

It must be noted that the measurement of the eye movement is not an EEG signal as the signal changes do not come from the brain's activity. However, as the amplitude of the moving eye is extremely high this measurement can be used to check the basic recording functionality of the circuit.

For this experiment the proband was told to move his eyes first upwards, then in a neutral position and after that downwards again. The signal was obtained once without a DRL attached to the user and once with a right leg electrode. Both recordings were then processed with a digital 50Hz notch filter and analyzed with a FFT. The same filter kernel as shown in Figure 6-5 was used for the processing. The results can be seen in Figure 6-12 - Figure 6-19.

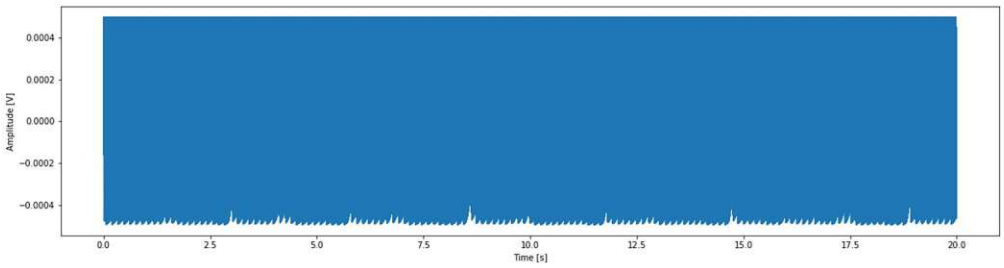

Figure 6-12 Recording of eye-movement without an attached DRL. The main hum is drowning the signal to a point where no movement can be discovered in the signal.

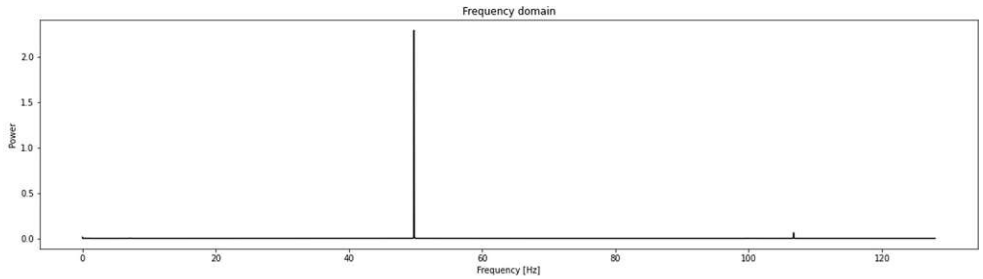

Figure 6-13 Power spectrum of eye-movement without an attached DRL. The 50Hz frequency is dominating the whole spectrum and no other frequencies can be quantified.

[50] (Cooper, Osselton, & Shaw, 1984), p. 103

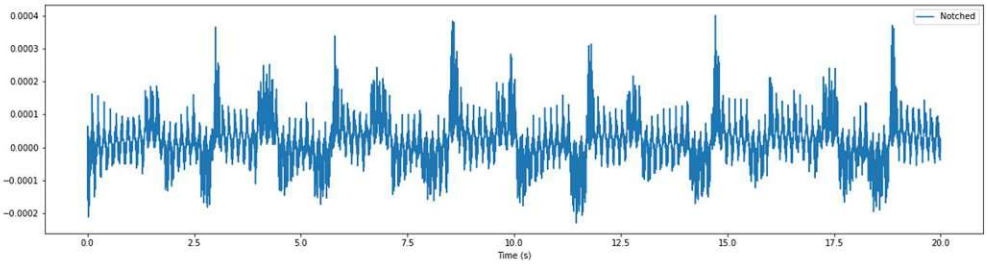

Figure 6-14 Recording of eye-movement without an attached DRL after a digital 50Hz notch filter was applied. The movement of the eye is starting to become visible but differentiating between up and downwards movements is not always possible.

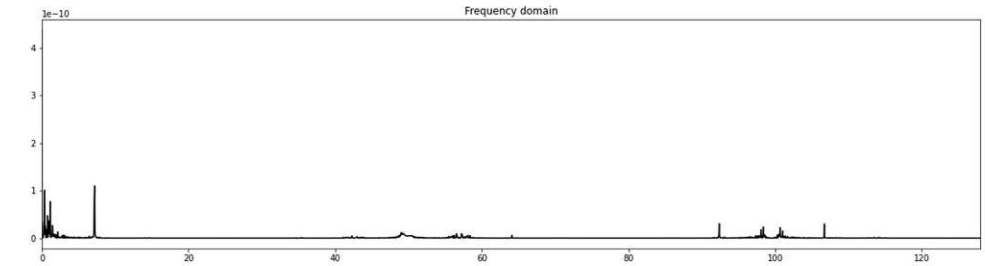

Figure 6-15 Power spectrum of eye-movement without an attached DRL after a digital 50Hz notch filter was applied. Although the filter was not able to completely suppress main hum, it was able to attenuate it to a level equal or smaller to the frequencies of interest.

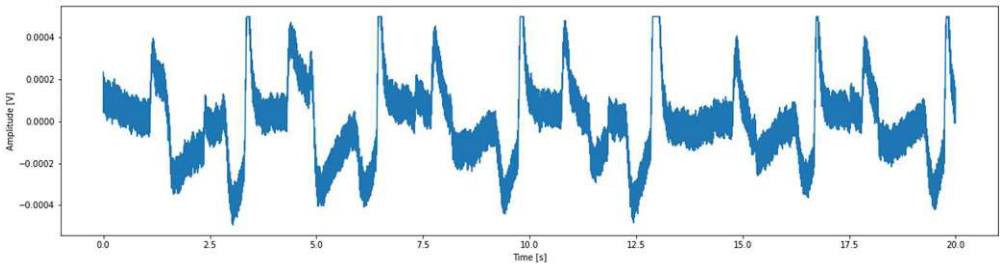

Figure 6-16 Recording of eye-movement with an attached DRL. Even though the power-line interferences are still very present in the signal, the eye-movements can be distinguished between an upwards (amplitude getting more positive before changing to negative) and downwards (amplitude getting more negative before changing to positive) movement.

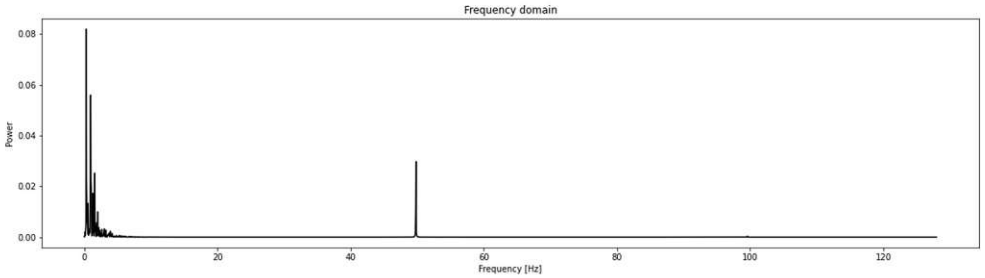

Figure 6-17 Analysis of the power spectrum of the eye-movement with an attached DRL. The main hum is still clearly visible at 50Hz but the rest of the signal in the lower frequency range is not drowned.

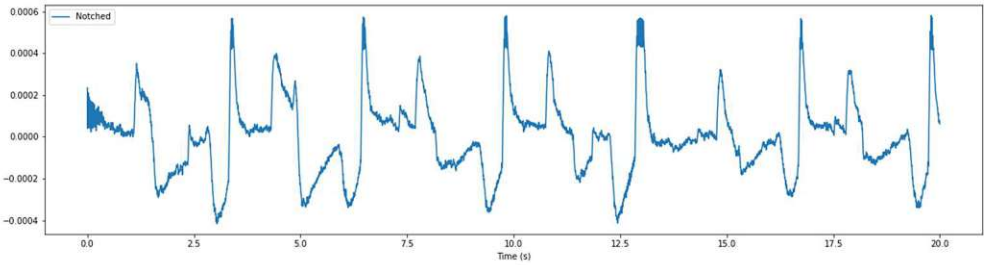

Figure 6-18 Combining a DRL while conducting the measurement of the eye-movement with a digitally applied 50Hz notch filter result in a clear and useful signal, where movement-directions can be distinguished.

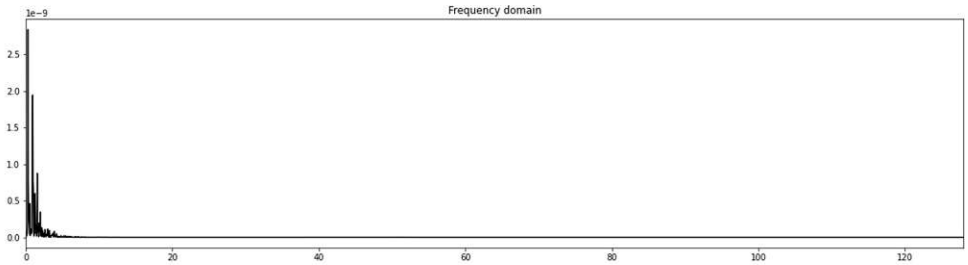

Figure 6-19 FFT analysis of the digitally filtered signal obtained with an DRL attached. No main hum is visible in the power spectrum anymore.

When looking Figure 6-14 and Figure 6-16 the reduction of noise when using a DRL or a digital notch filter can be seen quite well. However, the usage of a DRL has shown to be more effective in producing interpretable results then just using a notch filter on the unattenuated signal. Even though the signal produced by using a DRL is already showing the movement of the eyeballs, this result can be further improved by applying a 50Hz notch filter as seen in Figure 6-18. Here not only the movement of the eyes can be seen, but also the directions of the movement can be clearly distinguished. The direction of signal change is reversed for upwards and downwards movements. While the amplitude first increases and then decreases when looking upwards, it is reversed when looking downwards. This result is not surprising as the dipole of the eye is moved in the opposite direction but nevertheless can be used to differentiate between eye movement directions.

6.4 ALPHA WAVES

Alpha waves are oscillations in brain signals in the frequency range of 8-12Hz[51]. An increased proportion of alpha waves is associated with slight relaxation or relaxed alertness, with eyes closed. Hans Berger, the inventor of the EEG, was the first one to describe the existence of the alpha waves. He was particularly interested in "alpha blockage", which is the process by which alpha waves are replaced with beta waves after the subject opens his eyes. [52]

The center of the activity of alpha waves can be found in the occipital lobe, which sits at the back of the brain and is mainly responsible for the visual functioning of the human brain.[53] Therefore, the association with brain activity that occurs while the eyes are closed seems to be reasonable.

Conducting a measurement of the alpha waves with the EEG device I built turned out to be quite hard. The main problem introduced itself in the placement of the electrodes. As mentioned above the most prominent activity of alpha waves can be found in the occipital lobe which sits at the back of the head. Unfortunately, the electrode pads are not able to get good enough skin contact due to the hair present in this region. Using electrode gel turned out to be an insufficient solution as the electrodes would not self-adhere with the gel in place and a stable mechanism to hold the pads in position could not have been found.

Due to these limitations I tried to gather alpha waves signals from the FP1 and FP2 positions. This is suboptimal as the electrode placement is the furthest away from the occipital lobe. The proband was told to start with open eyes and then close his eyes after 5 seconds for a period of 10 seconds. To get a better look at the relevant frequency spectrum I digitally applied a range-pass filter from 8 Hz to 12 Hz.

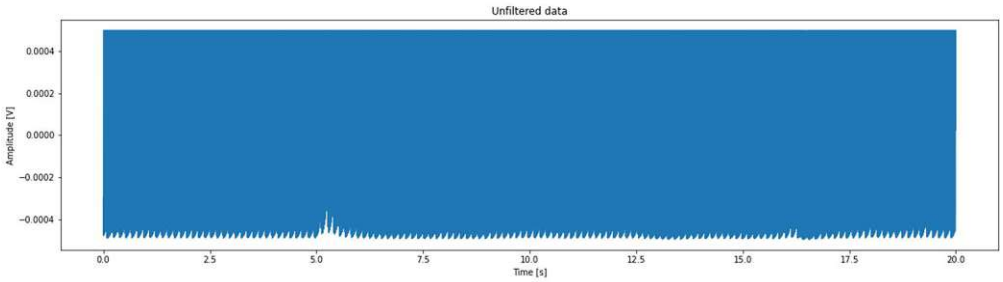

Figure 6-20 Time domain signal of the recorded Alpha-Waves without DRL and neither a 50Hz notch nor a 8-12Hz bandpass filter applied. At second 5 the artefact of the user closing his eyes can be seen.

[51] (Foster, Sutterer, Serences, Vogel, & Awh, 2017)

[52] (Subasi, 2019), p.30

[53] (Berger, 1929)

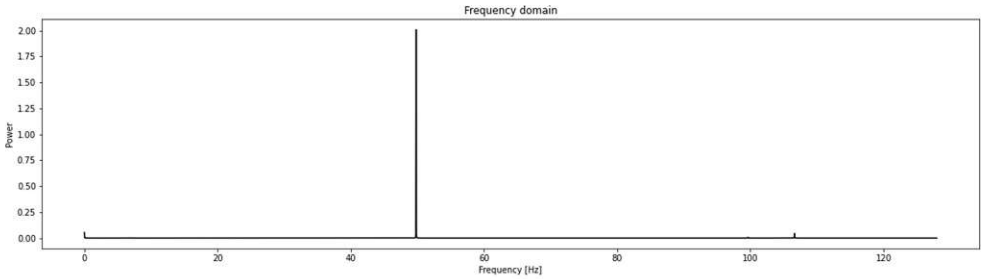

Figure 6-21 Power spectrum of the recorded alpha waves with no DRL and no digital filters applied. The main hum is again drowning any possible signal of interest

In Figure 6-20 and Figure 6-21 the signal and corresponding power spectrum without an applied DRL and no digital filters applied are shown, respectively. The interfering noise during the signal capturing was too high for even the possibility of alpha ways being visible. Only the blinking artefact of the user closing his eyes at second 5 stands out of the noise. When applying a 50Hz notch filter to the signal the blinking artefacts are even more prominent but still no alpha waves are detectable. This is shown in Figure 6-22 and Figure 6-23.

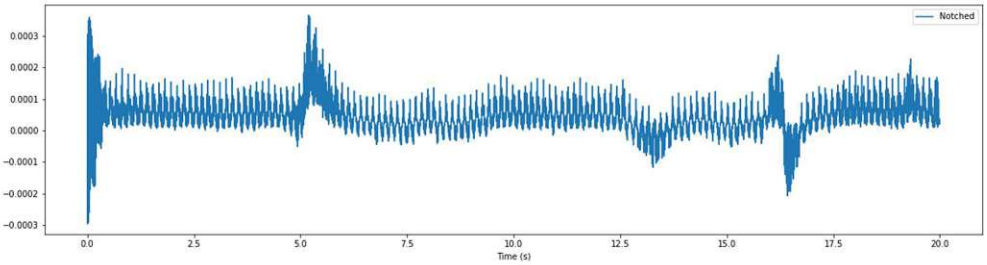

Figure 6-22 When a 50Hz notch filter is applied to the signal shown in Figure 6-20 the artefacts of closing and opening the eyes can clearly be seen. An increased activity during the period with closed eyes (seconds 5 to 16) can not be seen.

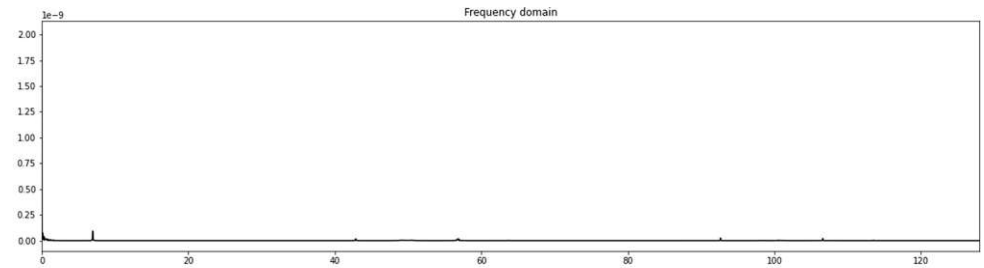

Figure 6-23 Power spectrum of the measurement as shown in Figure 6-21 with filtered power line frequencies. The majority of the frequencies lie in a narrow range close to 0Hz which implies that no significant signal of interest was recorded.

Narrowing the frequency spectrum further to a range from 8Hz to 12Hz the alpha waves, if present, should be clearly visible. There should especially be a significant difference between the signal with open eyes compared to closed eyes. The result of the band-pass-filter is shown in Figure 6-24. There is no difference in the signal's amplitude between 5 and 17 seconds, the time range where the user has closed his eyes, compared to the rest. Therefore, no alpha waves were detectable when

conducting the measurement without a DRL attached.

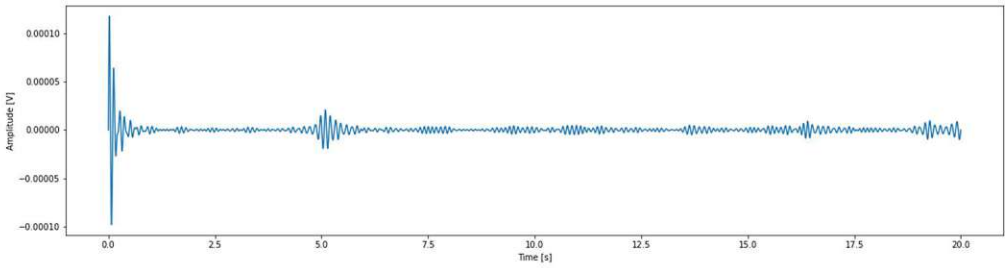

Figure 6-24 Time domain of the signal recorded without an attached DRL but with applied band-pass filter limiting the frequency range from 8Hz to 12Hz. Between second 5 and 17 the user had his eyes closed. No increase in amplitude is visible during this period.

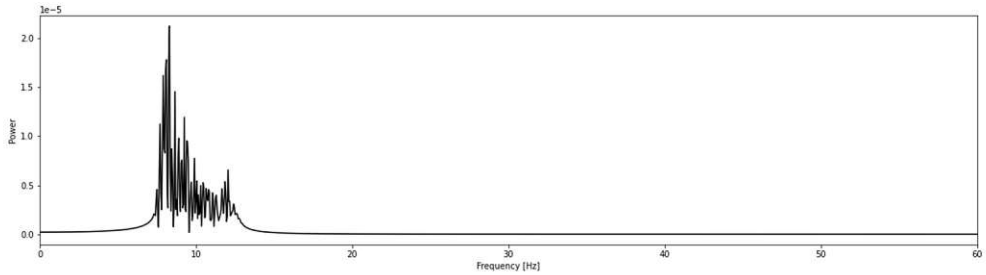

Figure 6-25 Power spectrum of the signal recorded without an attached DRL but with applied band-pass filter limiting the frequency range from 8Hz to 12Hz.

After not being able to detect alpha waves without a DRL, the measurement was repeated while the user was attached to the driven right leg circuit. The user closed his eyes at second 6 and opened it again at second 18. The results of this measurement are presented in Figure 6-26 and Figure 6-27.

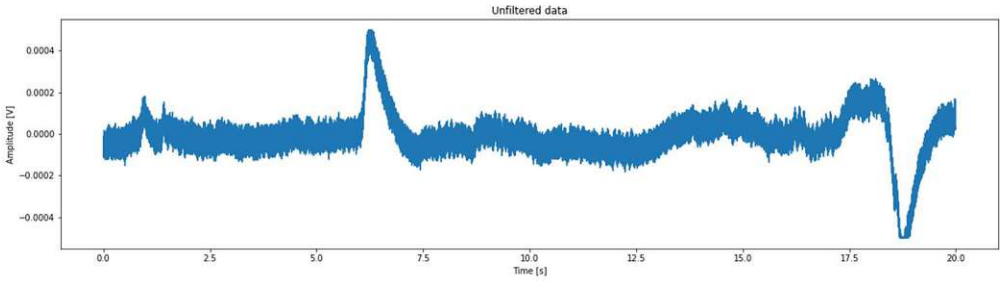

Figure 6-26 Time domain signal of the recorded Alpha-Waves with a DRL attached without digitally altering the recorded signal further. At seconds 6 and 18 the artefacts from opening and closing the eyes are visible.

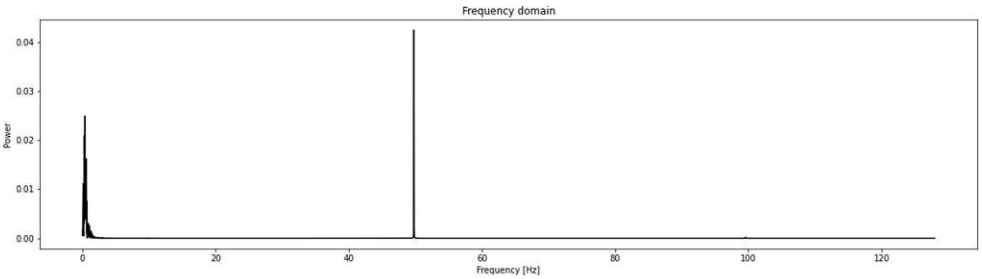

Figure 6-27 Power spectrum of the signal shown in Figure 6-26. Although the power line hum is noticeably reduced compared with the measurement without a DRL, the 50Hz domain is still the most prominent one.

Although the noise level is much reduced and the blinking artefacts produced by opening and closing the eyes can be seen clearly even without a digital filer applied, the period with closed eyes produced no visible difference in the signal's amplitude compared to when the user had his eyes opened. In Figure 6-27 the power line hum is still the main frequency domain present in the recorded signal and is probably masking every frequency range of interest. Applying an 8Hz-12Hz bandpass filter to the signal limits the power spectrum to the alpha waves range. In Figure 6-28 and Figure 6-29 the resulting signal is shown in the time and frequency domain.

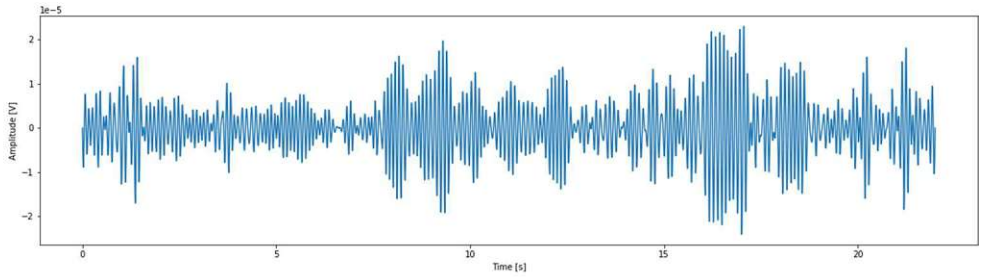

Figure 6-28 Time domain of signal recorded using a DRL and applying an 8Hz-12Hz bandpass filter. The user closed his eyes at 6 seconds and opened it again at 18 seconds. A slightly increased amplitude can be seen during this period.

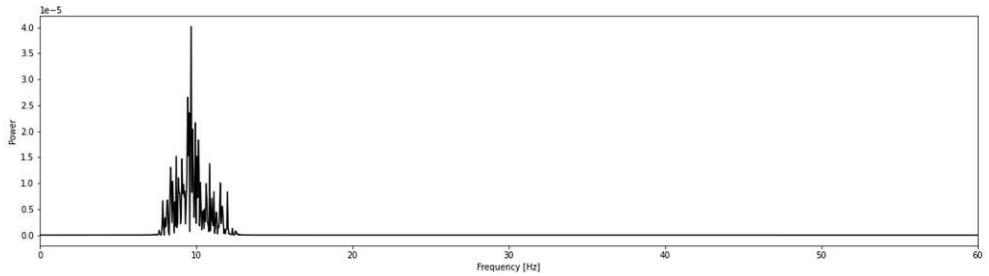

Figure 6-29 Power analysis of signal recorded using a DRL and applying an 8Hz-12Hz bandpass filter. The maximum frequency can be found at around 10Hz.

In Figure 6-28 a slight increase in amplitude can be seen during the period with closed eyes when compared to the signal with opened eyes. However, the increase is not significant enough to rule out it being an artefact or just coincident. Without having knowledge about the period where the eyes were closed it would be hard to make out the time range just by looking at the recorded signal.

To conclude the experiment, it can be stated that alpha waves were not able to be detected confidently using the EEG with electrodes placed at the FP1 and FP2 positions. Several reasons could cause this result. It could be that the low-cost ModularEEG is not sensitive enough to pick up the weak signals in the front of the brain. However, as other measurements done with medical grade equipment show that alpha waves are not very prominent with this electrode placement, the ModularEEG is not to be expected to show great results using this setup (see Figure 6-30). A more reasonable explanation is that a different type of electrodes is needed to conduct the measurements at positions O1 and O2 at the back of the head. Austin Griffith showed in his work with the ModularEEG that measuring the alpha waves is possible when the electrodes are placed correctly at O1 and O2.[54] He also described that he was not able to get any meaningful result in measuring the signal at FP1/FP2.

[54] (Griffith, 2006)

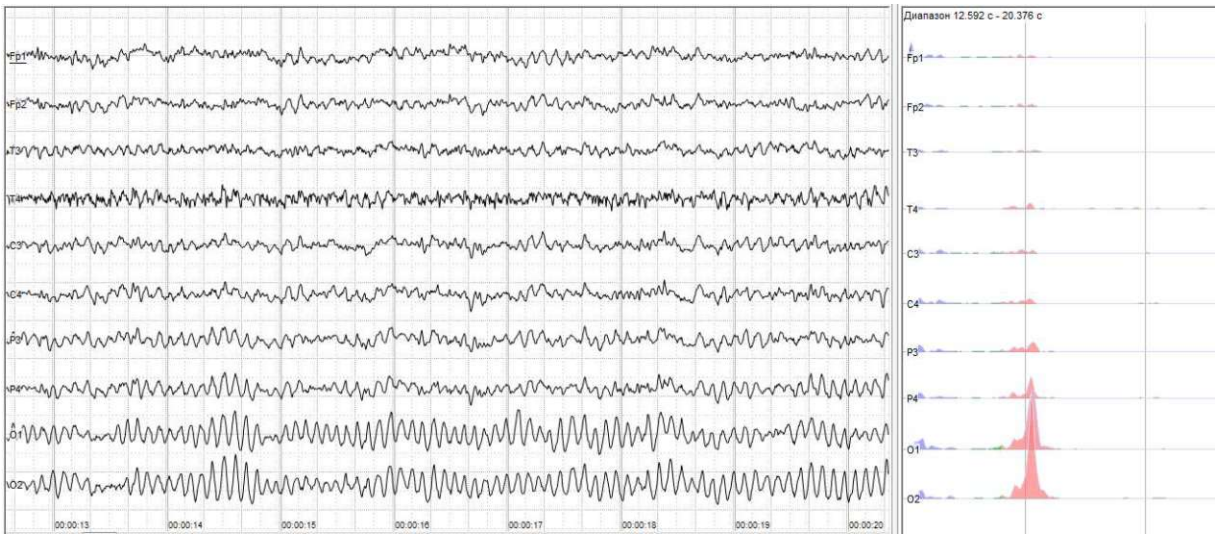

Figure 6-30 Human EEG with prominent resting state activity – alpha-rhythm. Left: EEG traces (horizontal – time in seconds; vertical – amplitudes, scale 100 µV). Right: power spectra of shown signals (vertical lines – 10 and 20 Hz, scale is linear). Alpha range is red at power spectrum graph. Almost no alpha waves can be detected at position Fp1 and Fp2 but are clearly visible at O1 and O2. From (Wikimedia, Andrii Cherninskyi, CC BY-SA 4.0, 2021)

6.5 MEASURING OTHER BIOSIGNALS

As an EEG device is nothing more than an extremely sensitive voltmeter it can be used to measure different biosignals as well. The ECG and EMG are of special interest in this regard.

6.5.1 ECG

The Electrocardiogram (ECG) is the measurement of the small electrical changes that are a direct consequence of cardiac muscle depolarization and repolarization occurring with each heartbeat. Therefore, an ECG can be especially useful to detect cardiac diseases and heart-rhythm disturbances.

The ECG signal can be categorized in three components: The P wave, representing the depolarization of the atria, the QRS complex, corresponding to the depolarization of the ventricles and the T wave, which shows the repolarization of the ventricles. [55]

In Figure 6-31 - Figure 6-36 the recorded signals of an ECG done with the ModularEEG are shown. As the amplitude of the ECG voltage is much higher compared to the EEG the amplification of the ModularEEG is maxing out the limits of the device. This makes it hard to categorize any components of the EEG signal as the peaks are out of limit. However, it is possible to derive the pulse frequency of the user and again show the effect of the usage of a DRL.

In Figure 6-32 the power spectrum of the recording without a DRL is shown. This reveals the dominance of the 50Hz frequency in the signal recorded, which is multiple magnitudes higher than the signal of interest in the lower frequency ranges. Again this can be filtered out using a digital 50Hz notch filter to improve signal's quality. In Figure 6-33 the filtered signal is shown. Cardoso et al.

[55] (Lilly, 2016)

showed that applying a 50Hz filter does not reduce the quality of a human ECG measurement.[56] Here the pulse's freuency can be determined to be 1.4 Hz which results in a pulse of 84BPM.

When comparing the digitally filtered signal with the DRL attenuated recording seen in Figure 6-35 and especially comparing the two power spectrums shown in Figure 6-34 and Figure 6-36 the power of a DRL can be shown quite well. While even after filtering out the 50Hz frequency in the measurment without a DRL, a bit of interfences can still be seen between 40Hz and 60Hz. Those are not present when a DRL is attached as the DRL is able to attenuate a common-mode signal independently of the actual frequency range.

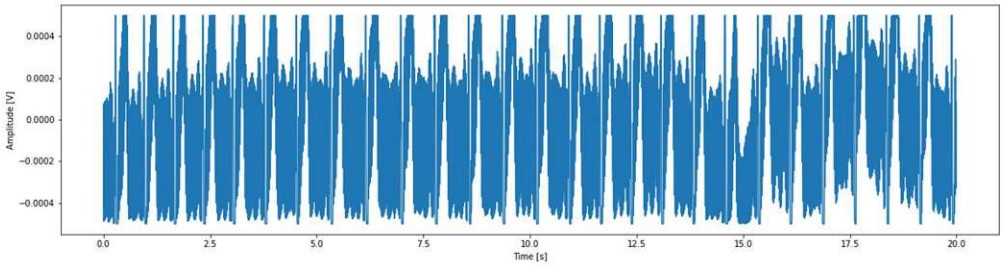

Figure 6-31 Time domain of the ECG without a DRL. The power line hum makes it impossible to identify the components of the ECG signal.

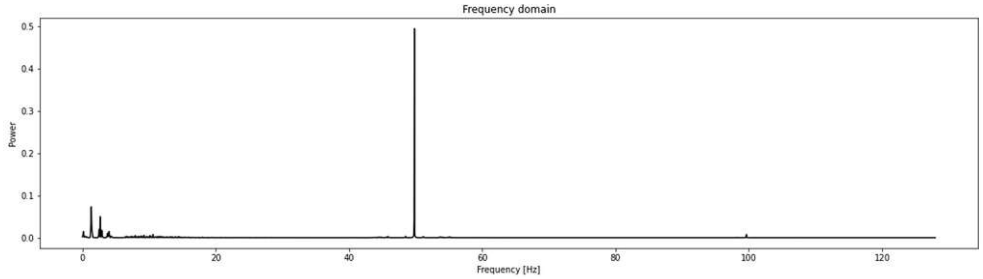

Figure 6-32 Frequency domain of the ECG recording without an attached DRL. The main hum is multiple magnitudes higher than the signal of interest in the lower frequency ranges.

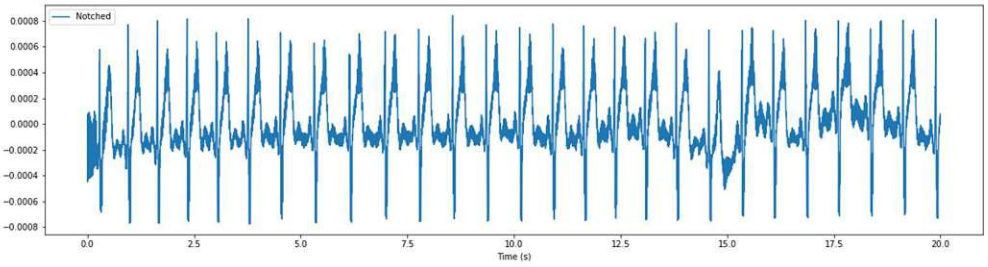

Figure 6-33 Time domain of the ECG without a DRL but with a 50Hz notch filter applied. The power line hum is not drowning the signal anymore but the QRS, P and T components of the EEG cannot be identified.

[56] (Cardoso, 2010)

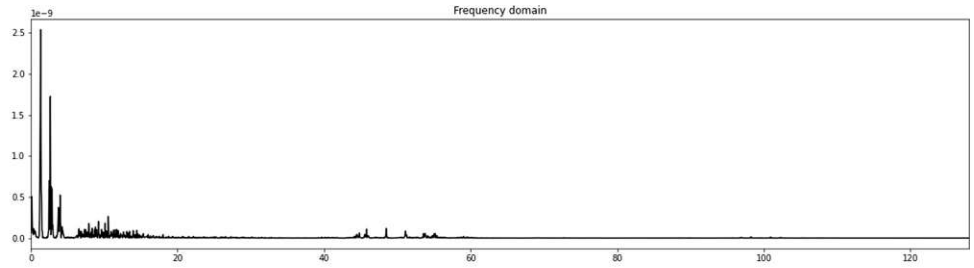

Figure 6-34 Frequency domain of the ECG without a DRL but with a 50Hz notch filter applied. The frequency range of interest is now the dominant one in the spectrum.

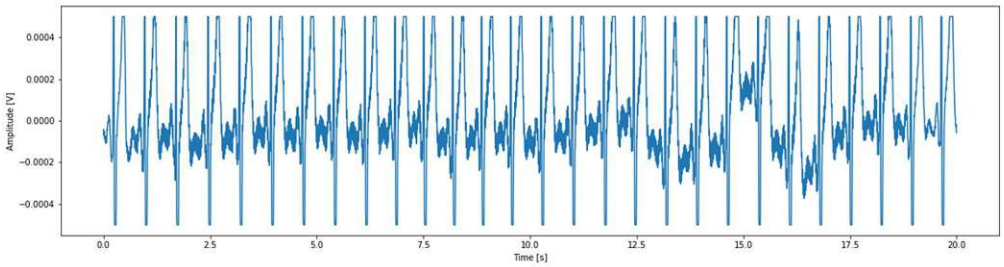

Figure 6-35 ECG recording with an attached DRL. As the amplitude of the ECG voltage is much higher compared to the EEG the amplification of the ModularEEG is too high and the signal is maxing out the limits of the device.

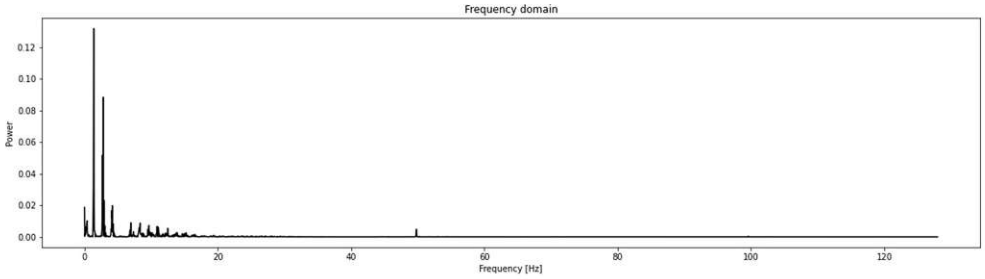

Figure 6-36 Power spectrum of the ECG recorded with an attached DRL. The amplitudes of the ECG signals are much higher than the induced power line hum.

6.5.2 EMG

An electromyogram shows the electrical activity of skeletal muscles while contracting. The signals can be analyzed to detect medical conditions, activation levels or recruitment order of animal or human movement.

For this thesis I tried to measure the muscular activity of biceps while contracted. Again, I repeated the measurements once with a DRL attached and once without it and applied a digital notch filter on both measurements. The results are shown in Figure 6-37 - Figure 6-44. When no digital filter is applied to the recordings, the interferences are drowning the signal both in the recording with a DRL and without a DRL attached. However, the usage of a DRL reduces the level of main hum induction enough to identify the contraction and relaxation timestamps in the recording. This is not possible when no DRL was used. After applying a digital 50Hz notch filter, the signal recorded with and without DRL differ significantly. When no DRL was attached a clear change in signal amplitude can be seen while the muscle was contracted. Interestingly this change was not present when a DRL was used. In this case it could be that driving the body potential using a DRL not only suppresses power

line inductions but also the recorded EMG in the body.

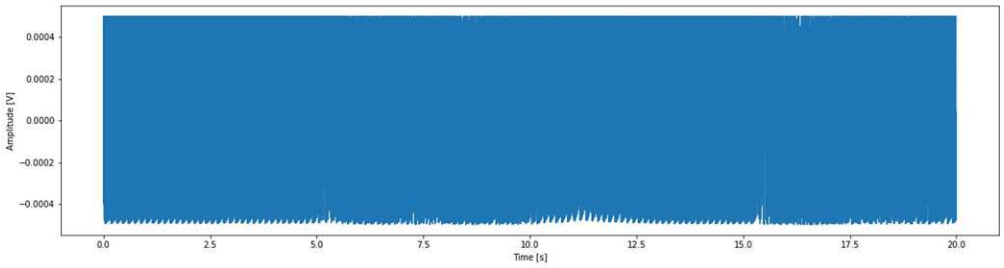

Figure 6-37 Recorded EMG on the biceps without a DRL attached. The power line hum masks every possible signal of interest.

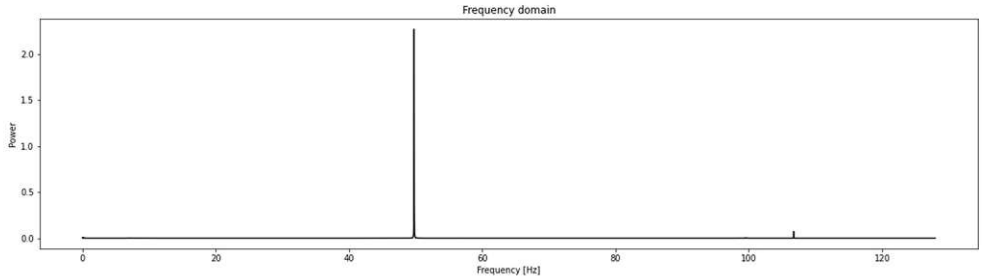

Figure 6-38 Power spectrum of an EMG recorded on the biceps without a DRL attached. The 50Hz frequency is too high for any other signal to be seen in the time domain.

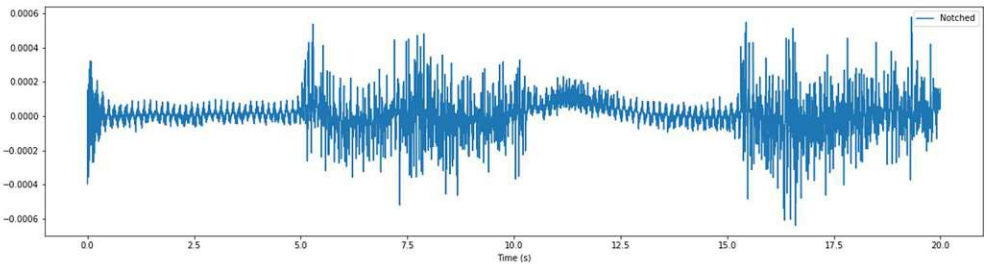

Figure 6-39 Time domain of a signal recorded on the biceps without a DRL attached after applying a 50Hz notch filter. The contraction of the muscle in the period 5s-10s and 15s-20s can be seen clearly.

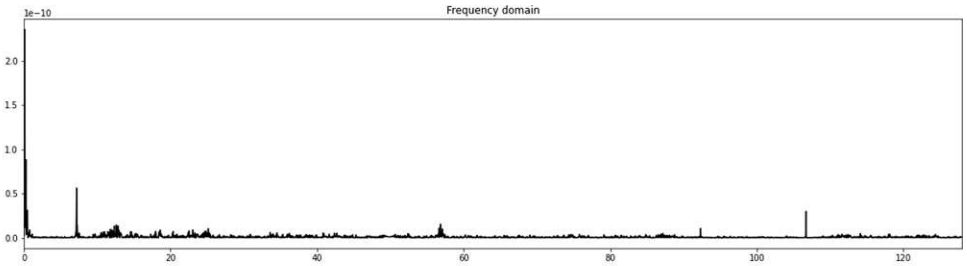

Figure 6-40 Frequency domain of EMG recorded on the biceps without a DRL after applying a 50Hz notch filter.

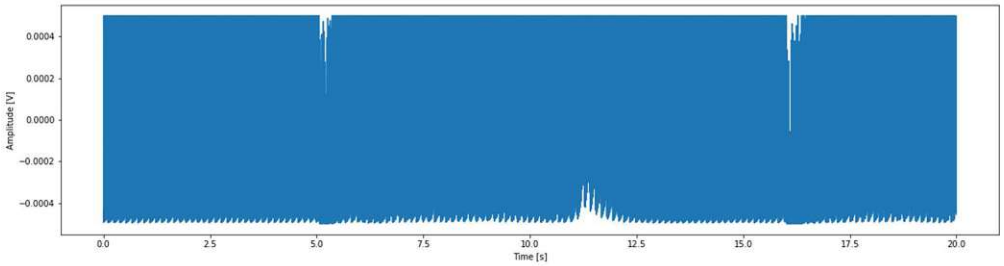

Figure 6-41 Recorded EMG on the biceps with a DRL attached. Even though the power line hum is the dominant part of the signal the artefacts when contracting at second 5 and second 16 as well as stopping the contraction at second 11 can be seen.

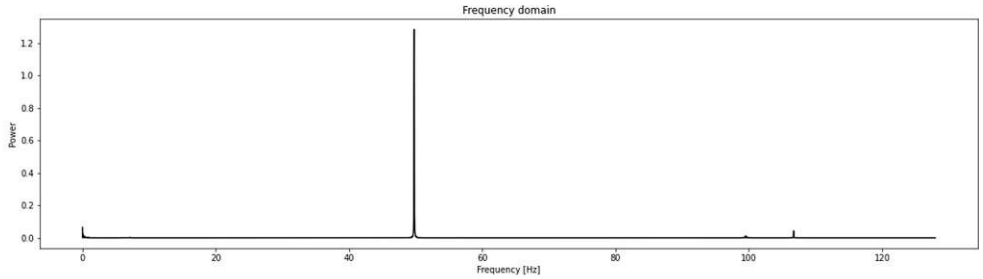

Figure 6-42 Frequency domain of EMG recorded on the biceps with a DRL attached. Even though the DRL attenuates 50Hz hum when compared to no DRL attached, it is still multiple times higher than any frequency of interest.

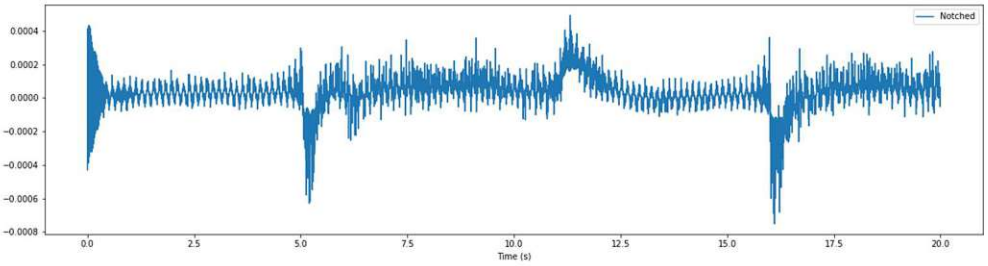

Figure 6-43 Time domain of a signal recorded on the biceps with a DRL attached after applying a 50Hz notch filter. Although a spike in the signal when contracting or relaxing the muscle is visible, the signals amplitude does not change during contraction.

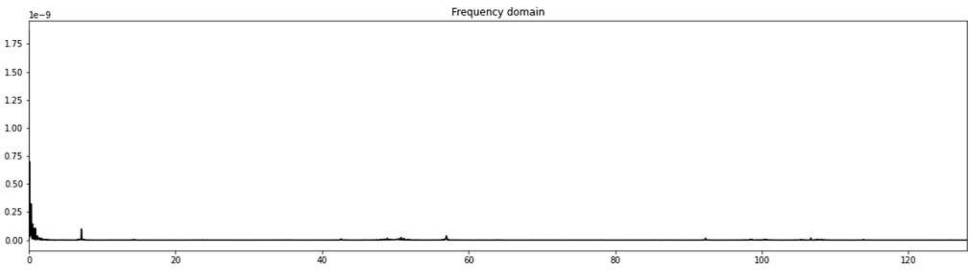

Figure 6-44 Frequency domain of EMG recorded on the biceps with a DRL after applying a 50Hz notch filter.

7 CONCLUSION

An EEG device is a powerful tool that can have many implications in research. Medical grade devices can cost more than 25000$ [57] and are not affordable for the home user. The OpenEEG project set out to be a low-cost EEG for the interested individual to get a glimpse into the fascinating world of measuring brain activity.

The design of the ModularEEG and the building tips on the site of the OpenEEG allows it even for not so experienced users to build their own EEG device for around 200-400€. The support of the company Olimex, which offers a great variety of products from PCBs to cables and even fully equipped PCBs, makes it even easier and more suitable for all pre-knowledge levels. This opens the world of brain computer interface development to thousands of independent home users and therefore contributes greatly to build up general interest in this topic.

The biggest problem I faced in the process of building an EEG device for this thesis was that a lot of the information on the OpenEEG project are outdated as the project started in the early 2000s and has not been active in the last years. However, there is a big mailing list archive available on the projects sourceforge page that allows to read up on other users discussing problems and maybe providing solutions.

Comparing the DRL method with a digital filtering technique with regard to the ability to suppress induced main hum offered a good insight into the capabilities and limitation of both of those techniques. With the exception of the EMG, where the DRL hindered the measuring process, it always turned out that it is best to combine a recorded signal with a DRL and a digital signal filter. However, if no DRL is available digitally filtering out the noise proved to deliver great results and is a capable method of improving signal quality.

Although I was not able to detect alpha waves using the ModularEEG I gained some remarkably interesting insights into the brain's functionality and the sensitive measuring techniques necessary to make neural activity visible. Also, I gained great knowledge about various topics regarding electronics and the communication between hardware and a PC.

To conclude, I can recommend building the ModularEEG for everyone who is interested in the minds activity and wants to have a nice project that can serve as an intro into advance electronics.

[57] (EEG Headset prices, 2021)

8 FURTHER IMPROVEMENTS

Although the ModularEEG built for this thesis provides a good basic starting point for measuring brain activity it can be further improved.

8.1 ELECTRODES

The electrodes are the most important part of the EEG to get a good signal quality. I decided to use passive electrodes as this thesis should be more about a proof of concept. However, in general I would recommend using active electrodes as the interfering noise was one the biggest problems when taking a measurement. Using active electrodes that have an amplifying circuit right at the electrode pad, the brains signal cannot be drowned that easily in noise while transmitting.

Furthermore, the electrodes could be improved by using a different design to reach through the hair onto the scalp. This could be done by either using cup electrodes that can be filled with gel and pressed against the head or by needle electrodes that have long comb-like spikes that can reach through the hair to the scalp. Joe Street proposed such a needle design to the OpenEEG project.[58]

8.2 MORE CHANNELS

The design of the ModularEEG is limited to a maximum of 4 channels if the ATMega8 microcontroller is used. This can be quite limiting while conducting experiments that need to have the whole brain region monitored. Medical grade devices can have up to 256 electrodes[59]. A design improvement for the ModularEEG proposed by Bastian Holtermann can implement up to 16 channels[60] by replacing the microcontroller and design new PCBs. This could lead to more complete results when conducting measurements.

[58] (OpenEEG Joe Street's active electrodes, 2021)

[59] (Lau, Gwin, & Ferris, 2012)

[60] (OpenEEG Diplomarbeit Holtermann, 2008)

9 REFERENCES

Berger, H. (1929). Über das Elektrenkephalogramm des Menschen. *Archiv für Psychiatrie und Nervenkrankheiten*, S. 527–570.

Cardoso, A. (01. 01 2010). The effect of 50/60 Hz notch filter application on human and rat ECG recordings. *Physiological measurement*.

Cooper, R., Osselton, J. W., & Shaw, J. C. (1984). *Elektroenzephalographie, Technik und Methoden* (3 Ausg.). Gustav Fischer Verlag.

Elsholz, M., Feser, M., & Trefzger, T. (2012). *Lehr-Lern-Labor Biophysik – Experimentieren im M!ND-Center Würzburg.* Didaktik der Physik.

Foster, J. J., Sutterer, D. W., Serences, J. T., Vogel, E. K., & Awh, E. (2017). Alpha-Band Oscillations Enable Spatially and Temporally Resolved Tracking of Covert Spatial Attention. *Psychological science*(28), S. 929-941.

Gertz, D., Schünke, M., & Liebman, M. (2003). *Basiswissen Neuroanatomie, leicht verständlich - knapp klinikbezogen* (4. Ausg.). Georg Thieme Verlag.

Griffith, A. (2006). An Exploration of the OpenEEG Project. *C.H.G.Wright's BioData Systems*.

Huhta, J., & Webster, J. (March 1973). 60-Hz Interference in Electrocardiography. *IEEE TRANSACTIONS ON BIOMEDICAL ENGINEERING, VOL. BME-20, NO. 2*.

Kandel, E. R., Schwartz, J. H., Jessell, T. M., Siegelbaum, S. A., & Hudspeth, A. J. (2012). *Principles of Neural Science.* McGraw-Hill Education.

Kirschstein, T. (2008). Wie entsteht das EEG? *Das Neurophysiologie-Labor*, S. 29-37.

Kryger, M. H., Roth, T., & Dement, W. C. (2011). *Principles and Practice of Sleep Medicine.* ScienceDirect.

Lau, T. M., Gwin, J. T., & Ferris, D. P. (31. May 2012). How Many Electrodes Are Really Needed for EEG-Based Mobile Brain Imaging? *Journal of Behavioral and Brain Science*, S. 387-393.

Lilly, L. S. (2016). *Pathophysiology of Heart Disease: A Collaborative Project of Medical Students and Faculty.* Lippincott Williams & Wilkins.

Nunez, P., & Srinivasan, R. (2006). *Electric fields of the brain - The neurophysics of EEG* (2. Ausg.). Oxford University Press.

Parks, T. W., & Burrus, C. S. (1987). *Digital Filter Design.* John Wiley & Sons.

Reece, J. B., Urry, L. A., Cain, M. L., Wasserman, S. A., Minorsky, P. V., & Jackson, R. B. (2014). *Campbell Biology, 10th Edition.* Pearson.

Schmidt, R. F., Lang, F., & Heckmann, M. (2004). *Physiologie des Menschen, mit Pathophysiolgie.* Springer Verlag.

Simon, O. (1977). *Das Elektroenzephalogramm, Einfuhrung und Atlas.* Urban & Schwarzenberg Verlag.

Smith, S. W. (1997). *The Scientist and Engineer's Guide to.* California Technical Pub.

Subasi, A. (2019). *Practical Guide for Biomedical Signals Analysis Using Machine Learning Techniques.* Academic Press.

Thakor, N., & Zhu, Y.-S. (1991). Applications of adaptive filtering to ECG analysis: noise cancellation and arrhythmia detection. *IEEE Transactions on Biomedical Engineering, vol. 38, no. 8*, S. 785-794.

Thompson, R. F. (1994). *Das Gehirn, Von der Nervenzelle zur Verhaltensteuerung.* Spektrum Akademischer Verlag.

Vaseghi, S. V. (2008). *Advanced digital signal processing and noise reduction.* John Wiley & Sons.

Wellach, I. (2020). *Praxisbuch EEG.* Thieme.

Wong, A., Pun, K.-P., Zhang, Y.-T., & Choy, C.-S. (2006). An ECG measurement IC using driven-right-leg circuit. *2006 IEEE International Symposium on Circuits and Systems*.

Wright, S. H. (December 2004). Generation of resting membrane potential. *Advances in Physiology Education*, S. 139-142.

Zschocke, S., & Hansen, H.-C. (2012). *Klinische Elektroenzephalographie.* Springer-Verlag.

10 ONLINE REFERENCES

EEG Headset prices. (2021). Von https://imotions.com/blog/eeg-headset-prices/ abgerufen

ModularEEG analogue board schematics. (2003). Von http://openeeg.sourceforge.net/doc/modeeg/modEEGamp-v1.0.png abgerufen

ModularEEG Building instructions. (2021). Von http://openeeg.sourceforge.net/doc/modeeg/modeeg_building.html abgerufen

ModularEEG digital board schematics. (2003). Von http://openeeg.sourceforge.net/doc/modeeg/modEEGdigital-v1.0.png abgerufen

Olimex OpenEEG. (2021). Von https://www.olimex.com/Products/EEG/OpenEEG/ abgerufen

OpenEEG design documentation. (2021). Von http://openeeg.sourceforge.net/doc/modeeg/modeeg_design.html abgerufen

OpenEEG Diplomarbeit Holtermann. (2008). Von http://openeeg.sourceforge.net/doc/modeeg/Modification/modeeg16/Diplomarbeit.pdf abgerufen

OpenEEG Joe Street's active electrodes. (2021). Von http://openeeg.sourceforge.net/doc/hw/joe_ae/ abgerufen

OpenEEG Project page. (2021). Von http://openeeg.sourceforge.net/doc/ abgerufen

Sourceforge project OpenEEG. (2021). Von https://sourceforge.net/projects/openeeg/ abgerufen

Wikimedia, Andrii Cherninskyi, CC BY-SA 4.0. (2021). Von https://commons.wikimedia.org/wiki/File:Human_EEG_with_prominent_alpha-rhythm.png abgerufen